



Research paper

Discovery of novel Thymol-TPP antibiotics that eradicate MRSA persisters

Ziyi Tang^{a,1}, Jizhou Feng^{b,1}, Mahesh Challa^b, Sankara Rao Rowthu^b, Shuxin Xiong^b, Cheng Zou^b, Jianguo Li^{c,d}, Chandra Shekhar Verma^{d,e,f}, Haibo Peng^g, Xiaoli He^a, Chao Huang^{b,**}, Yun He^{b,h,*}

^a Chongqing Institute of Green and Intelligent Technology, Chinese Academy of Sciences, Chongqing, 400714, China

^b Chongqing Key Laboratory of Natural Product Synthesis and Drug Research, School of Pharmaceutical Sciences, Chongqing University, Chongqing, 401331, China

^c Singapore Eye Research Institute, Singapore, 169856, Singapore

^d Bioinformatics Institute, A*STAR, 30 Biopolis Street, Matrix, 138671, Singapore

^e Department of Biological Sciences, National University of Singapore, 117543, Singapore

^f School of Biological Sciences, Nanyang Technological University, 637551, Singapore

^g Chongqing Academy of Science and Technology, Chongqing, 401123, China

^h BayRay Innovation Center, Shenzhen Bay Laboratory, Shenzhen, 518132, China

ARTICLE INFO

Keywords:

Antibacterial

Thymol

Triphenylphosphonium (TPP)-conjugates

Persister

ABSTRACT

The high prevalence of methicillin-resistant *Staphylococcus aureus* (MRSA) strains and the formation of non-growing, dormant "persisters" subsets help bacteria evade antibiotic treatment and enhance bacterial resistance, which poses a serious threat to human life and health. It is urgent to discover novel antibacterial therapies effective against MRSA persisters. Thymol is a common nutraceutical with weak antibacterial and antitumor activities. A series of Thymol triphenylphosphine (TPP) conjugates (TPP-Thy3) was designed and synthesized. These compounds showed significantly improved inhibitory activity against Gram-positive bacteria compared with Thymol. Among them, Thy3d displayed a low probability of resistance selection and showed excellent biocompatibility. Interestingly, Thy3d elicited a rapid killing effect of MRSA persisters (99.999%) at high concentration. Fluorescence experiments, electron microscopy, molecular dynamics simulation and bilayer experiment confirmed that Thy3d conjugates exerted potent antimicrobial activity by disrupting the integrity of the membrane of bacterial even the persister. Furthermore, Thy3d exhibited considerable efficacy in a mouse model of subcutaneous murine MRSA infection. In summary, TPP-Thy3 conjugates are a series of novel antibacterial agents and could serve as a new therapeutic strategy for combating antibiotic resistance.

1. Introduction

Since the discovery of penicillin in 1928, antibiotics have become the most commonly used drugs for treating a variety of infections, and the widespread use of antibiotics has saved billions of patients' lives and extended human being's life for 15–20 years on average. However, the abuse and misuse of antibiotics have led to a drastic increase in bacterial resistance, posing a serious threat to public health [1]. Bacterial persisters, a small phenotype mutation subgroup, are often in a dormant, or inactive state, and can tolerate lethal concentrations of antibiotics and thus escape antibiotic treatment, leading to enhanced bacterial

resistance [2]. Bacterial persisters play a critical role in perpetuating chronic and recurrent infections, which can not be treated with conventional antibiotics [3,4]. Hence, the development of novel antimicrobial agents effective for treating resistant bacterial persisters is urgently needed.

However, few compounds have been reported with activity against persister cells [5]. Therefore, addressing drug resistance by eliminating persisters has become a research hotspot worldwide. Three strategies have been put forward to eliminate persisters [2]. One approach seeks to directly kill metabolically dormant persister cells [6,7]. An alternative approach sensitizes the persister cells for conventional antibiotics

* Corresponding author. Chongqing Key Laboratory of Natural Product Synthesis and Drug Research, School of Pharmaceutical Sciences, Chongqing University, Chongqing, 401331, China.

** Corresponding author.

E-mail addresses: chuang@cqu.edu.cn (C. Huang), yun.he@cqu.edu.cn (Y. He).

¹ Z.Y. Tang and J.Z. Feng contributed equally to this study.

through resuscitation, activating the antibiotic targets, or stimulating the antibiotic influx [8,9]. The third approach employs molecules to disrupt or reduce the formation of persister cells. Triphenylphosphonium cation (TPP^+), a lipophilic cation, can easily cross lipid bilayers due to its high lipophilicity and stable cationic charge, and the potential gradient drives the accumulation of TPP^+ -conjugates in the mitochondrial matrix [10]. There have been reports on the conjugation of TPP^+ with drugs to improve their anticancer efficacy by increasing their distribution in the mitochondria [11,12]. Since the bacterial cell wall is a phospholipid bilayer, TPP-conjugates could potentially cross the bacterial cell wall via similar interactions, accumulating in the bacterial cytoplasm and leading to an enhanced antibacterial effect [13,14]. For example, the TPP-linked prodrugs ciprofloxacin-ester- PPh_3 and ciprofloxacin-amide- PPh_3 induced significant morphological changes in MRSA ST5 5016, including irregular deformation and membrane disruption, and some leakage of the cytoplasmic contents of bacteria to the extracellular environment [14]. Based on the membrane permeability of TPP^+ , we hypothesized that conjugation of TPP^+ with natural products could further enhance its antibacterial activities, and have the potential to directly destroy persister cells.

Thymol is a naturally occurring phenolic monoterpene, which is one of the major constituents of the essential oils (10–64%) of thyme (*Thymus vulgaris* L., Lamiaceae), a medicinal plant with multiple therapeutic properties [15]. Thymol exhibits antimicrobial, antioxidant, anticarcinogenesis, anti-inflammatory, and antispasmodic activities, as well as a potential as a growth enhancer and immunomodulator [16]. However, due to the high concentrations required to reach therapeutic effects, the efficiency of Thymol in clinical applications was limited. Continuing our studies on novel antibiotic discovery [13,17–23], we set out to conduct Structure-Activity Relationship (SAR) studies on Thymol in the hope of improving its antibacterial activity.

We synthesized a series of derivatives by introducing a substituent to the 4-position of Thymol. Antibacterial evaluation of these derivatives against the priority bacteria (*Staphylococcus aureus*, *Klebsiella pneumoniae*, *Acinetobacter baumannii*, *Pseudomonas aeruginosa*, and *Enterobacter* species) as defined by WHO identified derivatives with significantly improved antibacterial activities. We then selected the potent Thymol derivatives to form conjugates with TPP^+ , and further studied their SAR and antibacterial activities, leading to the discovery of Thymol-TPP conjugates effective against bacterial persisters. We also established their preliminary antibacterial mechanisms. The strategy reported in this study could help develop novel antibiotics to address the drug resistance challenges, from natural products that are often neglected in traditional bioassays due to their weak antibacterial activity.

2. Results and discussion

2.1. Synthesis of Thymol derivatives and TPP conjugates

The synthesis of designed Thymol derivatives **Thy1–4** is shown in Scheme 1. Commercially available Thymol reacted with SOCl_2 in CH_2Cl_2 to afford 4-chloro-2-isopropyl-5-methylphenol (**Thy1**), and TBABr_3 in $\text{MeOH}/\text{CH}_2\text{Cl}_2$ (v/v, 2:3) to afford 4-bromo-2-isopropyl-5-methylphenol

(**Thy2**). Suzuki coupling of **Thy2** with boronic acids in $\text{EtOH}/\text{Toluene}/\text{H}_2\text{O}$ (v/v/v, 2/2/1) produced **Thy3** and **Thy4**.

The synthesis of Thymol derivatives **Thy5–27** is shown in Scheme 2. The target compounds were obtained in good yields via Suzuki coupling of **Thy2** with various boronic acids.

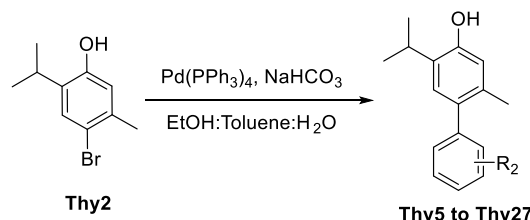
The synthesis of TPP-conjugates was started with bromoalkyl acid by reacting with PPh_3 in acetonitrile to obtain (carboxyalkyl) triphenylphosphonium bromides, which then reacted with the corresponding Thymol derivative **Thy3** to afford the TPP-conjugates via Steglich Esterification (Scheme 3).

The general synthetic route for these compounds is presented in Schemes 1–3. All spectral and analytical data of the newly synthesized compounds were in full agreement with the proposed structures (Extended Data Fig. 1).

2.2. In vitro antibacterial activity of thymol derivatives and TPP-conjugates

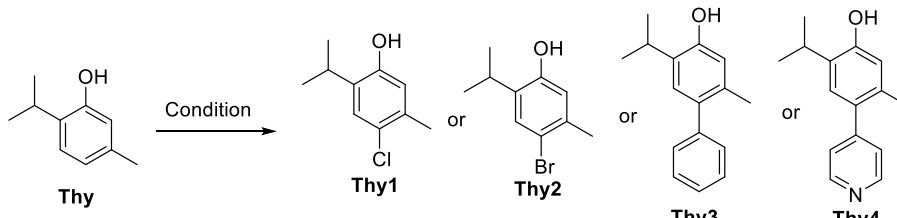
The ESKAPE bacteria are priority pathogens to fight against [24]. In our study, several Gram-positive bacteria (*S. aureus* ATCC 43300, MRSA USA 300, MRSA 3390) and Gram-negative bacteria (*E. coli* ATCC 25922, *E. coli* 53328, *P. aeruginosa* ATCC 27853, *P. aeruginosa* 535, *K. pneumonia* ATCC 700603, *K. pneumonia* 3026, *A. baumannii* ATCC 19606 and *A. baumannii* 1318) were selected as test bacteria in our studies. Thymol derivatives **Thy1–4**, **Thy5–27**, and **Thy3a–3i** were first evaluated for their *in vitro* antibacterial activity against these bacteria through the double dilution method, using ciprofloxacin as the positive control (Tables 1–3 and Extended Data Tables 1–2).

For the first series of Thymol derivatives (**Thy1**, **Thy2**, and **Thy4**), most displayed moderate to weak *in vitro* antibacterial activity against all tested Gram-positive bacteria, with only about a 4–8 fold increase in

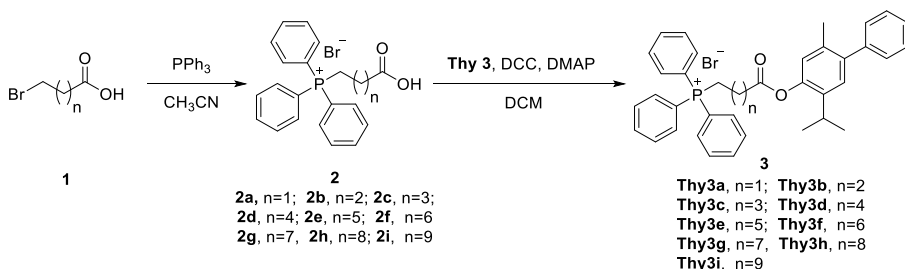


R_2	R_2	R_2
Thy5	Thy13	Thy21
$2'\text{-OCH}_3$	$2'\text{-F}$	$4'\text{-COOH}$
Thy6	Thy14	Thy22
$3'\text{-OCH}_3$	$3'\text{-F}$	Thy23
Thy7	Thy15	$3'\text{-CN}$
$4'\text{-OCH}_3$	$4'\text{-F}$	Thy24
Thy8	Thy16	$4'\text{-Cl}$
$3'\text{-OH}$	Thy17	Thy25
Thy9	$3'\text{-Cl}$	Thy26
$4'\text{-OH}$	Thy18	$3'\text{-CF}_3$
Thy10	$4'\text{-Cl}$	Thy27
$2'\text{-CH}_3$	Thy19	$3'\text{-COOH}$
Thy11	$2'\text{-COOH}$	
$3'\text{-CH}_3$	Thy20	$3'\text{-COOH}$
$4'\text{-CH}_3$		

Scheme 2. Synthesis of **Thy5–Thy27**.



Scheme 1. Synthesis of **Thy1–Thy4**. Reaction conditions and reagents: for **Thy1**, SOCl_2 , CH_2Cl_2 ; for **Thy2**, TBABr_3 , $\text{CH}_3\text{OH}/\text{CH}_2\text{Cl}_2$ (v/v, 2/3); for **Thy3** and **Thy4**, $\text{Pd}(\text{PPh}_3)_4$, NaHCO_3 , $\text{EtOH}/\text{Toluene}/\text{H}_2\text{O}$ (v/v/v, 2/2/1). Thy means Thymol.



Scheme 3. Synthesis of TPP-conjugates Thy3a-Thy3i.

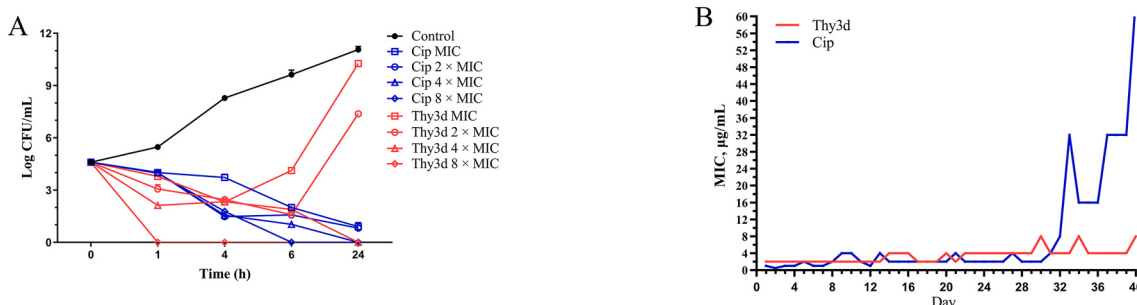


Fig. 1. Time-kill kinetic, and bacterial resistance of Thy3d. (A) Time-kill assay of Thy3d against MRSA 3390. Data are mean \pm SD for $n = 3$ biologically independent samples. (B) MRSA 3390 evolution under Thy3d and ciprofloxacin stress over 40 days of serial passages. Cip = Ciprofloxacin.

Table 1

Antibacterial activity of Thymol derivatives (Thy1-4) against Gram-positive strains.

Comp.	Structure	MIC ($\mu\text{g}/\text{mL}$)		
		S. <i>a</i> ATCC 330041	MRSA USA 300	MRSA 3390
Thy		128	128	256
Thy1		64	64	64
Thy2		64	64	32
Thy3		16	8	16
Thy4		128	128	128
Cip	-	2	1	1

Thy = Thymol, MIC = Minimum inhibitory concentration. Cip = Ciprofloxacin. S. *a* = *S. aureus*.

antimicrobial activity compared to Thymol (Table 1). However, Thy3 exhibited significantly improved antibacterial activity against *S. aureus* (MIC = 8–16 $\mu\text{g}/\text{mL}$), which was about 8–32 times more potent than natural Thymol, and thus was selected for further optimization. However, Thy1-4 had no detectable antimicrobial activity against Gram-negative bacteria at concentrations up to 64 $\mu\text{g}/\text{mL}$ (Extended Data Table 1).

Starting from Thy3, we further designed and synthesized the second series of Thymol derivatives (Scheme 2) and evaluated their antibacterial activities (Table 2 and Extended Data Table 2). Most of these derivatives maintained good antibacterial activity against Gram-positive

S. aureus and MRSA, with MIC values less than 16 $\mu\text{g}/\text{mL}$ except for Thy5 and Thy9. Compared with Thy3, some compounds, such as Thy25–27, showed slightly improved antibacterial activity (Table 2). However, similar to Thy3, none of these compounds displayed antibacterial activity against Gram-negative bacteria (Extended Data Table 2). SAR analysis suggested that electron-donating substituents on the phenyl group (Thy5–12) led to reduced activity in comparison with Thy3, while a methyl substituent at the C-2 or C-4 position of the phenyl ring (Thy10, Thy12) exhibited similar antibacterial activity (8 $\mu\text{g}/\text{mL}$). In contrast, derivatives with electron-withdrawing groups on the phenyl ring (Thy13–27) displayed a 7–30 fold improvement over Thymol, which is similar to or better than Thy3. Compounds with 3'-F (Thy14), 2'-Cl (Thy17), and 3'-COOH (Thy20) on the phenyl ring were similar to Thy3 in terms of their antimicrobial activity, and derivatives with 3'-Cl (Thy17) and CF₃ (Thy25–27) on the phenyl ring showed a 2-fold improvement over Thy3. Introduction of Cl to the phenyl ring (Thy16–18), their antibacterial activity was in the order of meta > para > ortho. However, the introduction of CF₃ on the phenyl ring had a similar effect on their antibacterial activities, regardless of its position on the phenyl ring (Thy25–27).

It has been reported that TPP⁺ conjugated with a cationic charge could interact with negatively charged cell membranes more easily through electrostatic interaction, thus affecting bacterial cell permeability. For example, TPP⁺-CL conjugates were membrane-targeting compounds, which can disrupt bacterial cell membrane integrity, thus with enhanced antibacterial efficacies to combat the CL resistance strains [13]. We hypothesized that the conjugation of TPP with Thymol derivatives might enhance the permeability of these derivatives across bacterial membranes, leading to improved antibacterial potency and broad antibacterial ranges. Thus, we designed and synthesized a series of TPP conjugates linking Thy3 to the lipophilic cation (carboxyalkyl) triphenylphosphonium with varying linker chain lengths (Scheme 3). Antibacterial evaluations (Table 3) identified TPP conjugates (Thy3a-3i) as the most potent compounds against MRSA with MICs lower than 2 $\mu\text{g}/\text{mL}$, which are 4–16 folds more potent than Thy3, about 100 folds more potent than natural Thymol. The antibacterial activities of Thy3a-3i against MRSA were essentially the same (MIC = 0.5–2

Table 2

Antibacterial activity of Thymol derivatives (Thy5-27) against Gram-positive strains.

Comp.	Structure	MIC ($\mu\text{g/mL}$)			Comp.	Structure	MIC ($\mu\text{g/mL}$)		
		<i>S. a</i> ATCC 330041	MRSA USA 300	MRSA 3390			<i>S. a</i> ATCC 330041	MRSA USA 300	MRSA 3390
Thy5		>64	>64	>64	Thy17		4	8	8
Thy6		16	16	16	Thy18		8	4	8
Thy7		16	32	16	Thy19		16	8	8
Thy8		32	32	32	Thy20		8	8	16
Thy9		>64	>64	>64	Thy21		16	16	8
Thy10		8	8	16	Thy22		16	8	8
Thy11		16	8	8	Thy23		32	16	8
Thy12		8	16	8	Thy24		16	16	32
Thy13		8	16	16	Thy25		8	8	16
Thy14		16	16	16	Thy26		8	4	8
Thy15		16	16	16	Thy27		4	4	8
Thy16		8	8	8	Cip	-	0.5	1	2

MIC = Minimum inhibitory concentration. MRSA = methicillin-resistant *S. aureus*. Cip = Ciprofloxacin. *S. a* = *S. aureus*.

Table 3

Antibacterial activity of TPP-Thymol conjugates (Thy3a-3i).													
Comp.	n	MIC ($\mu\text{g/mL}$)	Gram-positive bacteria			Gram-negative bacteria							
			S. a ATCC 330041	MRSA USA 300	MRSA 3390	E. coli ATCC 25922	E. coli 53328	P. a ATCC 27853	P. a 535	K. p ATCC 700603	K. p 3026	A. b ATCC 19609	A. b 1318
Thy3a	1	1	1	0.5	4	>64	>64	>64	32	>64	32	32	16
Thy3b	2	2	2	1	16	16	64	>64	16	32	8	8	8
Thy3c	3	1	1	1	16	8	>64	>64	32	32	16	8	8
Thy3d	4	1	0.5	1	8	8	32	64	8	16	8	8	8
Thy3e	5	1	1	1	8	8	>64	>64	8	8	8	8	8
Thy3f	6	2	0.5	1	4	8	32	32	16	16	8	16	16
Thy3g	7	1	2	1	4	16	64	32	64	64	16	8	8
Thy3h	8	2	1	1	4	64	32	32	32	>64	32	16	16
Thy3i	9	2	2	1	>64	32	64	>64	>64	>64	>64	>64	>64
Cip	-	0.5	1	2	0.06	0.12	1	1	0.12	0.06	0.5	1	

MIC = Minimum inhibitory concentration. MRSA = methicillin-resistant *S. aureus*. Cip = Ciprofloxacin, *S. a* = *S. aureus*. *P. a* = *P. aeruginosa*. *K. p* = *K. pneumonia*. *A. b* = *A. baumannii*.

$\mu\text{g/mL}$), regardless of the chain length. Furthermore, **Thy3d-3h** displayed good inhibitory activity against all tested Gram-negative bacterial strains except for *P. aeruginosa*. Unlike the report by Khailova. et al. [25], the antibacterial activity of the Thymol derivatives did not correlate with the chain length. When the chain length is $n = 4-8$, it exerts strong and broad-spectrum antibacterial activities.

In our studies, the MIC value of Thymol against *S. aureus* was about 100–200 $\mu\text{g/mL}$ (Table 1), and no antibacterial activity was detected against Gram-negative bacteria (Extended Data Table 1). After modification of Thymol, **Thy3-TPP** series compounds showed similar activity to the positive control ciprofloxacin, displaying excellent antibacterial activity against Gram-positive bacteria, with MIC at about 1 $\mu\text{g/mL}$ (Table 3). Compared with Thymol, antibacterial activity was increased more than 100 times. Unlike Thymol, most **Thy3-TPP** compounds also showed good antibacterial effects against multidrug-resistant Gram-negative bacteria (Table 3). The above results demonstrated that, the antibacterial ability of compounds can be significantly improved after conjugation with the TPP⁺ group, providing a strategy for the design and modification of compounds in the future.

2.3. In vitro cytotoxicity study

TPP-conjugated compounds with the ability to destroy cell membranes usually have a small therapeutic window, most likely due to their non-specific cell membrane damage to bacteria and normal cells, which is a limiting factor in application potential as antibiotics [26]. We evaluated the cytotoxicity of **Thy3** and **Thy3a-Thy3i** against L02 cells (normal human liver-02) by MTT assay to evaluate their *in vitro* safety. As shown in Table 4 and Extended Data Fig. 2, the cytotoxicity of these conjugates varied significantly. Conjugates **Thy3a**, **Thy3b**, **Thy3c**, **Thy3h**, and **Thy3i** showed higher toxicity than parent Thymol derivative **Thy3**, while the rest displayed reduced toxicity. **Thy3d** showed significantly lower toxicity than **Thy3**, with an IC₅₀ = 34.26 $\mu\text{g/mL}$ (Table 4), representing the largest toxicity-activity window among the conjugates, and thus was selected to explore its antibacterial mechanism.

2.4. Time kill kinetics of **Thy3d**

To determine the conditions for further biological evaluations, a kill-time assay was carried out with the compound **Thy3d** (Fig. 1A). At a concentration of $2 \times \text{MIC}$, a $\geq 2 \log_{10}$ reduction against MRSA was observed in 4 h. However, the initial killing was not sustained, with bacterial re-growth after 24 h. Application of a higher concentration ($4 \times \text{MIC}$) resulted in a $\geq 2 \log_{10}$ reduction in 1 h. Furthermore, the antibacterial activity of **Thy3d** at $4 \times \text{MIC}$ was sustained over 24 h. At the highest concentration tested ($8 \times \text{MIC}$), bacteria were eliminated after treatment for 1 h, and the bactericidal activity was sustained for 24 h. Ciprofloxacin inhibited bacterial growth at a lower concentration with an MIC (2 $\mu\text{g/mL}$) for a short time. Higher concentrations ($4-8 \times \text{MIC}$) of ciprofloxacin resulted in sustained bactericidal activity against MRSA for 24 h, which was similar to that of **Thy3d**. Taken together, **Thy3d** exhibited a rapid bactericidal effect, killing MRSA in a concentration- and time-dependent manner.

2.5. Resistance development study

The development of resistance is a great challenge that hampers antibiotic development and the eradication of nosocomial pathogens. We evaluated the selection of resistance through serial passaging in the presence of sub-inhibitory concentrations of **Thy3d** or ciprofloxacin up to 40 passages (Fig. 1B). With the exposure to ciprofloxacin, it showed no significant change in the first 30 generations, but then exhibited obvious resistance, with a 100-fold increase in MIC after 40 passages. However, no significant change was observed for **Thy3d**, with only a 4-fold change after 40 passages. The above results indicate a low tendency for bacterial resistance with **Thy3d**. Since cell membrane synthesis involves complex biochemical processes, membrane-targeted antibacterial compounds generally have a low drug resistance [27]. We speculate that **Thy3d** delays the emergence of resistance possibly due to the membrane-targeting function of the TPP moiety.

Table 4
IC₅₀ of **Thy3**, and **Thy3a-Thy3i**.

Compounds	Thy3	Thy3a	Thy3b	Thy3c	Thy3d	Thy3e	Thy3f	Thy3g	Thy3h	Thy3i
IC ₅₀ ($\mu\text{g/mL}$)	13.46	7.96	5.04	8.31	34.26	18.82	21.13	13.16	8.67	3.13

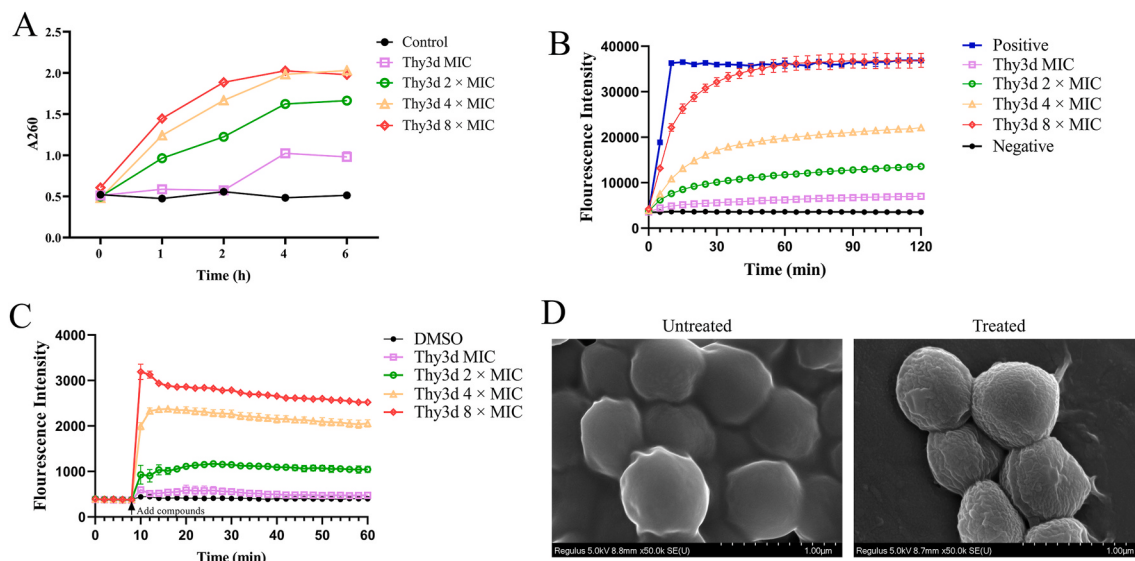


Fig. 2. The mode of action of **Thy3d** on MRSA 3390. (A) Leakage of 260 nm absorbing material of MRSA 3390 treated with different concentrations of **Thy3d**. (B) Membrane permeabilization assay in MRSA 3390 monitoring uptake of SYTOX™ Green of **Thy3d**. (C) Membrane depolarization assay in MRSA 3390 monitoring uptake of DiSC₃(5) of **Thy3d**. (A), (B), and (C), data are mean \pm SD for n = 3 biologically independent samples. (D) Scanning electron micrographs showing bacterial cell membrane structures in 4 × MIC **Thy3d** treated (right) cells and DMSO control (left). Scale bars, 1 μ m.

2.6. Effect of **Thy3d** on the bacterial cell membrane

Thy3d contains a TPP group, which was reported to disrupt cell membranes [10,28]. We thus explored whether **Thy3d** exerted its antibacterial effect by disrupting the bacterial cell membrane as we designed.

Consistent with our hypothesis, **Thy3d** caused DNA leakage, membrane permeabilization, and membrane depolarization in MRSA 3390 (Fig. 2). Since nucleic acid leakage can be used as an index of membrane permeability, we measured the absorption of **Thy3d** at 260 nm (Fig. 2A) [29]. For all treatment groups, the absorption at 260 nm reached the peak after 4 h and remained at a similar level after that. The absorption intensity at 260 nm increased with time and concentration compared with the control group. This result showed that **Thy3d** can disrupt cell membrane. Fluorescent probes SYTOX™ and DiSC₃(5) were used to detect membrane integrity and membrane potential changes of bacteria, respectively. The fluorescence intensity of SYTOX™ reached the peak within 5 min and remained at this level at the end of our test (Fig. 2B). As shown in Fig. 2C, the treated groups at MIC, 2 × MIC, 4 × MIC, and 8 × MIC showed induction of fluorescence compared to the control group, and all treated groups reached a steady state after 10 min (monitored by DiSC₃(5) assays uptake). The results indicate that the permeabilization and depolarization of the cell membrane of MRSA by the **Thy3d** was time- and dose-dependent.

SEM was used to further investigate the change in cellular morphology after membrane damage caused by **Thy3d**. A comparison of treated versus untreated MRSA 3390 reveals a significant difference in membrane morphology. In the absence of **Thy3d**, the bacteria appeared normal with intact and smooth surfaces. However, **Thy3d** destroyed the plasma membrane, and the tested bacteria showed rough, shrunken, and wrinkled surfaces (Fig. 2D). These results support that **Thy3d** exerts its bactericidal effect by damaging the bacterial cell membrane.

2.7. Mechanism of **Thy3d** with biomembranes

All the above studies indicate that **Thy3d** is a membrane-active compound. However, its mechanism of interaction with the membrane is still unknown. To elucidate the molecular interactions between **Thy3d** and the bacterial cell membrane lipid bilayers, we employed molecular dynamics (MD) simulations to investigate the effects of **Thy3d** binding

on the lipid bilayer organization [30], and electrical recording experiments to elucidate its mode of action in *S. aureus* [31].

As shown in Fig. 3A, after simulation of the trajectory, **Thy3d** prefers to stay at the head group region, with the polar moiety interacting with the head groups and the hydrophobic moiety inserting into the lipid tail region of the membrane. The perturbation of the membrane-water interface destabilizes the membrane. With the extension of simulation time, the membrane interaction of **Thy3d** remained essentially unchanged. In addition, we also simulated the interaction of **Thy3d** with the mammalian membrane (Extended Data Fig. 3), the mechanism of action is similar to that of the bacterial cell membrane. However, while **Thy3d** can penetrate either bacterial membrane or mammalian membrane, it penetrates deeper into the bacterial membrane (Fig. 3B). Furthermore, we compared the free energy of **Thy3d** on two different cell membranes (Fig. 3C). Free energy simulations suggest that **Thy3d** is more favorable to penetrate the bacterial membrane and experiences less energy barrier to penetrate bacterial membrane than mammalian membrane. This result is consistent with its strong antibacterial ability (Table 3) and weak cytotoxicity (Table 4) of **Thy3d**. The MD simulation results suggest that **Thy3d** may enhance the structural fluctuation within the water-lipid interface, and exert bacterial membrane damage. However, due to energy preference, mammalian cell membranes are less affected and therefore exhibit weak cytotoxicity.

To validate the MD simulation results, we carried out a series of experiments to explore the interactions between **Thy3d** and the lipid bilayer. 12 μ g/mL of **Thy3d** was added and stirred in the chamber, after the formation of a lipid bilayer in an orifice on a Teflon film [31]. The ionic current began to fluctuate significantly around 4 min (Fig. 3D), indicating that due to the strong interaction, **Thy3d** started to breach the membrane. During the next 4 min, the ionic current rapidly went up to a peak value (Fig. 3D), suggesting that the continuous lipid extraction had passed the critical point ($t \approx 4.7$ min) and the pore formation in the lipid bilayer became possible. Applying an equal volume of DMSO, the ionic current remained unchanged at 0 pA (Extended Data Fig. 4), suggesting a stable and unbroken lipid bilayer. Overall, these experimental observations are consistent with the simulations that **Thy3d** exerts its antibacterial ability mainly by infiltrating and penetrating cell membrane lipid bilayers.

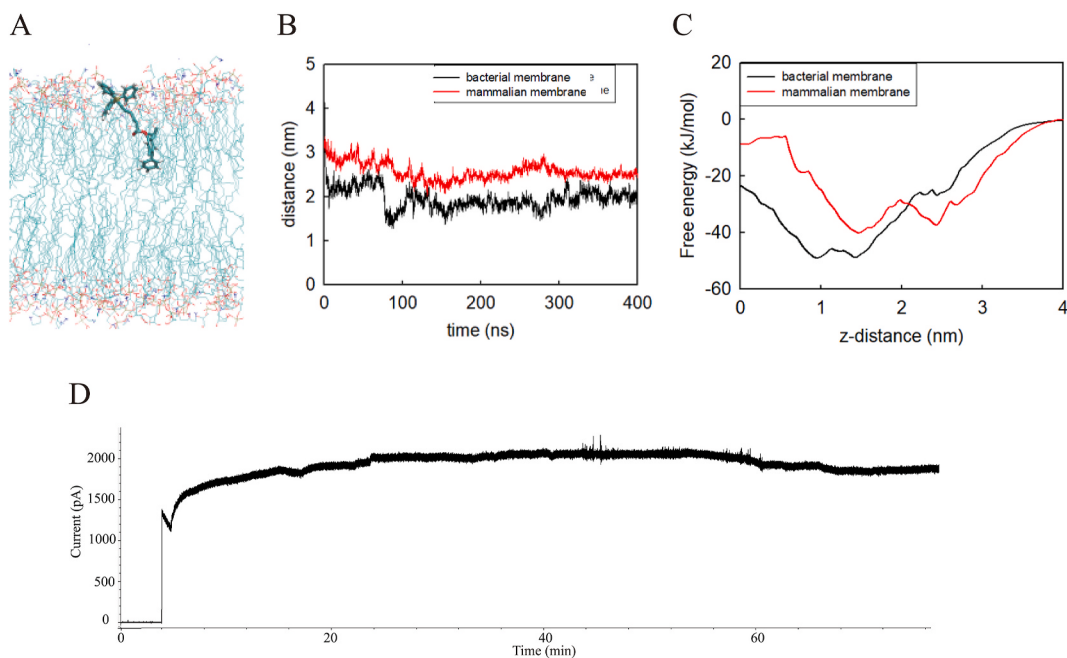


Fig. 3. Studies on the interactions between Thy3d and the lipid bilayer. (A) Representative configurations of molecular dynamics simulations of Thy3d in bacterial membrane. (B) Distance of lipid in the bilayers in the bacterial or mammalian membrane in the MD simulations. (C) Free energy of Thy3d adsorption from the aqueous phase to the membrane phase constructed by umbrella sampling. The distance between the bilayer center and the center of mass of the compounds (z-distance) was used as the reaction coordinate. All simulations were repeated three times. (D) Experimental studies on interactions between Thy3d and the lipid bilayer. The experiment was performed at +100 mV with the lipid bilayer formed on a Teflon film. The electrolyte solution contains 1 M KCl, 10 mM Tris, and 1 mM EDTA (pH 7.6). n = 2 biologically independent experiments.

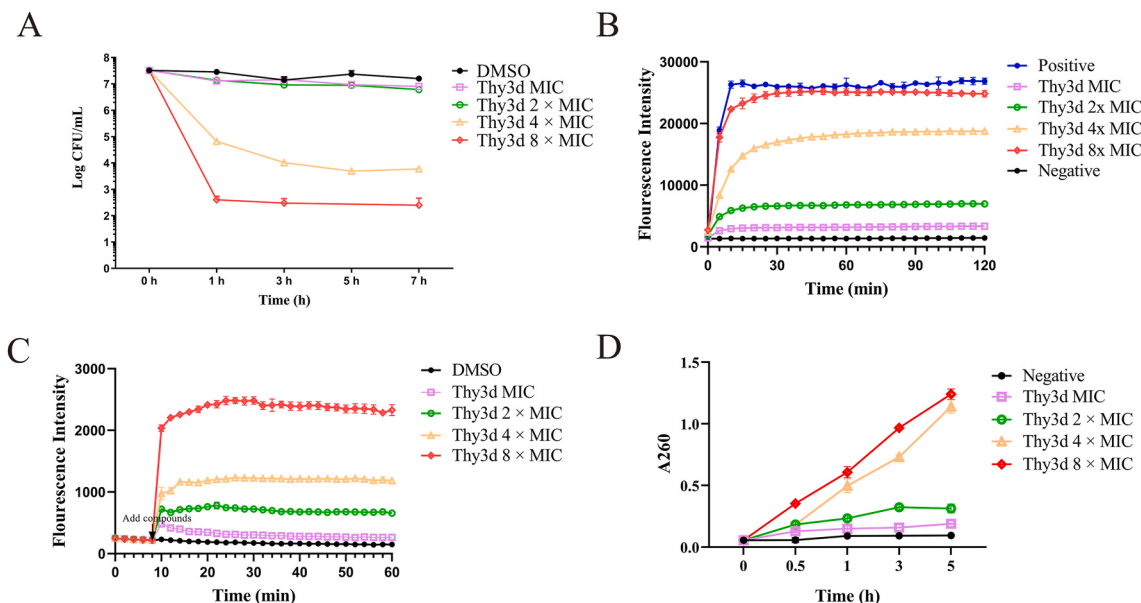


Fig. 4. The killing effect of Thy3d on persister of MRSA. (A) Eradication of persister by Thy3d. (B) Membrane permeabilization assay for persisters, monitoring uptake of SYTOX_{TM} Green of Thy3d. (C) Membrane depolarization assay for persisters, monitoring uptake of DiSC₃(5) of Thy3d. (D) Leakage of 260 nm absorbing material of persister cells treated with different concentrations of Thy3d. (A), (B), (C), and (D), data are mean \pm SD for n = 3 biologically independent experiments. The strain is MRSA 3390.

2.8. Eradicating MRSA persisters by Thy3d

Due to the dormant state of persisters, it can tolerate lethal concentrations of antibacterial drugs, which help bacteria evade antibiotic treatment [32]. Previous studies suggest that small molecules capable of destroying bacterial cell membranes might be effective against bacterial persisters and in overcoming bacterial resistance [3,33,34]. Thy3d

demonstrated potent inhibitory activity against MRSA, as well as targeting the cell membrane. We speculated that Thy3d, which destroys normal bacterial cell membranes, might also remove persisters. Thus its ability to eradicate MRSA persistence was further evaluated.

When treated with 4–8 \times MIC of Thy3d (4–8 μ g/mL), the number of persisters decreased sharply over time (Fig. 4A). Thy3d at its 4 \times MIC and 8 \times MIC elicited a rapid killing effect of 4 and 5 log units (99.99%

and 99.999%). Furthermore, the rapid killing of MRSA persisters with 4 × and 8 × MIC of **Thy3d** was sustained for 7 h, indicating that **Thy3d** is very effective in killing persister cells.

The killing effect of **Thy3d** on the persisters may be due to its rapid penetration of MRSA-persister membranes. When treated with 4–8 × MIC **Thy3d** (4–8 µg/mL) against MRSA persister, the membrane permeability (Fig. 4B) and membrane potential (Fig. 4C) of the persisters changed significantly in a short time, reaching the peak within 30 min and 10 min respectively, and then maintaining the high fluorescence intensity. These results indicate that **Thy3d** can rapidly disrupt the cell membrane of the persister at high concentrations, causing DNA leakage (Fig. 4D), which plays an important role in eliminating the persisters. MD experiments suggest that **Thy3d** can penetrate the membrane more efficiently owing to the lower energy barriers, which are more favorable for transferring energies (Fig. 3B). These results are consistent with the observation that **Thy3d** is effective against persister cells. In the above exploration of the persistent bacteria, we found that the destruction effect of **Thy3d** on normal bacterial cell membranes also extended to the persistent bacteria, exerting the same membrane-breaking ability on persister membranes, effectively removing the persisters.

2.9. *In vivo* efficacy of **Thy3d** in mouse subcutaneous infection model

We next established bioluminescent *S. aureus* Xen29 infection in a mouse topical infection model and evaluated the potential therapeutic application of **Thy3d** in the model.

In the saline group and **Thy3d** treated group, the fluorescence intensity of *S. aureus* Xen29 showed a dynamic pattern. There was a gradual increase in the early stage of infection and then a gradual decrease. Throughout the experiment, the fluorescence intensity of the **Thy3d** group and infection group began to appear different at 24 h, and **Thy3d** led to a significant reduction of fluorescence intensity ($p = 0.0155$ for **Thy3d** vs. vehicle) until 84 h (Fig. 5A and B), and wound scabbing was noticeably improved. The number of colonies at infection was also reduced by about 10 times in the **Thy3d** group compared to the saline group (Fig. 5C). Though **Thy3d** was not as effective as the positive control ($P = 0.0176$ for vancomycin vs. vehicle) (Fig. 5). These results suggest that **Thy3d** has a certain influence on the development of subcutaneous infection. The weight loss exhibited by the mice during infection was significantly reduced when compared with saline controls and positive controls, suggesting a favorable safety property (Extended Data Fig. 5).

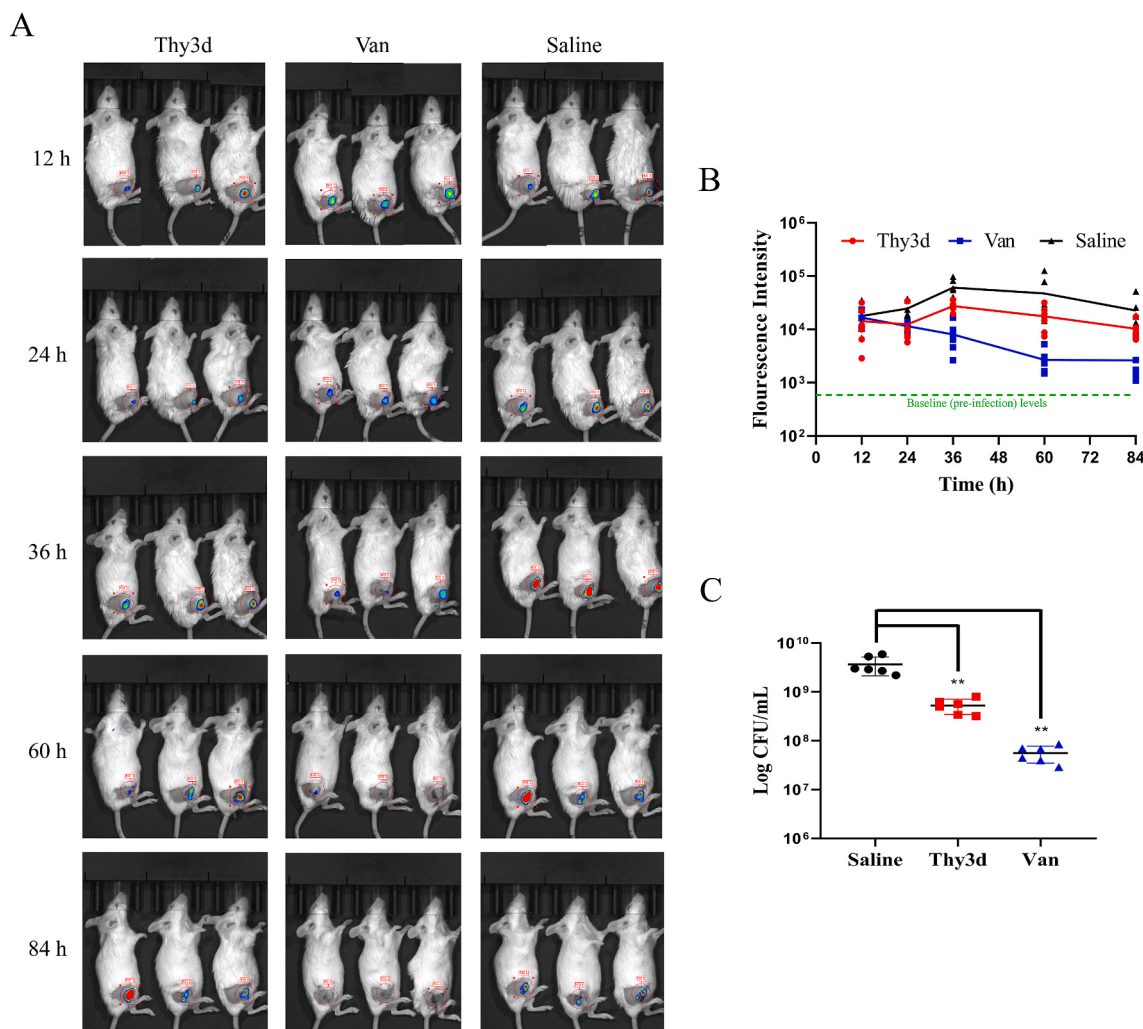


Fig. 5. *In vivo* efficacy studies of **Thy3d** in topical skin infection model. (A) Animals were imaged using the Lumina II system (PerkinElmer) at 12, 24, 36, 60, and 84 h post-infection (only 3 mice shown per image) and (B) bioluminescence (photons per second) was determined. (C) At 84 h after the first treatment and infection, animals were sacrificed and samples of skin from each animal were homogenized and plated on nutrient agar to determine the CFUs per animal. Errors are mean ± SEM, $n = 6$ animals. Statistical differences between control and antibiotic treatment groups were analyzed by t-tests (* $p < 0.05$) compared with the indicative group.

3. Conclusions

A series of novel antibiotics was designed and synthesized based on widely applied natural Thymol, whose antibacterial activity was improved by nearly 100 times. These derivatives exhibited a significantly broader antibacterial spectrum, with potent activities against several ESKAPE pathogens.

The TPP-Thymol derivatives exert their antibacterial property by targeting bacterial membranes, displaying fast killing and low probability of resistance development. In particular, **Thy3d** effectively eradicates MRSA persister cells. Mechanistic studies suggested that **Thy3d** could enhance the structural fluctuation within the water-lipid interface, infiltrate and penetrate lipid bilayers, and disrupt bacterial cell membranes, directly killing normal as well as persistent bacteria. Meanwhile, due to its free-energy preference, **Thy3d** has a higher affinity for bacterial cell membranes, thus **Thy3d** exhibited low toxicity for normal cells while maintaining potent activities for both normal and persister bacteria. While previous studies on TPP moiety mainly focused on anti-tumor activity [10,35], our results demonstrate TPP conjugates could be designed to discover novel antibiotics against Gram-positive, Gram-negative as well as persister bacteria. Our studies support that natural products are still an important source for novel antibiotic discovery, and our work provides a new strategy to fight the threatening antibiotic resistance, particularly those caused by bacterial persisters which have no effective treatment to date.

4. Materials and methods

4.1. Synthesis

4.1.1. General remarks

All chemicals were purchased from a commercial source and used without further purification unless otherwise stated. The reactions were monitored by thin-layer chromatography. Column chromatography was performed on silica gel. ^1H NMR spectra were obtained on an Agilent 400 MR spectrometer, while ^{13}C NMR spectra were obtained with proton decoupling on an Agilent 400 MR DD2 (100 MHz) or 600 MR DD2 spectrometer and were reported in ppm with residual solvent for internal standard (δ 77.16 (CDCl_3)). The chemical shifts were reported in parts per million (ppm), the coupling constants (J) were expressed in hertz (Hz) and signals were described as singlet (s), doublet (d), triplet (t), as well as multiplet (m). The NMR data was analyzed by MestReNova software. High-resolution mass spectra were obtained on a Bruker SolariX 7.0 T spectrometer. The purity of all test compounds was determined to be >95% by HPLC. All other chemicals and solvents were commercially available and were used as received.

4.1.2. 4-Chloro-2-isopropyl-5-methylphenol (**Thy1**)

To a solution of Thy (1 eq.) in DCM, was added a solution of SO_2Cl_2 (1.2 eq.) in DCM at 0 °C, and the mixture was stirred at room temperature for 2 h. After the reaction completion, the solvent was concentrated under reduced pressure, the crude residue was purified by silica gel chromatography to afford **Thy1**. ^1H NMR (600 MHz, CDCl_3) δ 7.15 (s, 1H), 6.62 (s, 1H), 4.82 (bs, 1H), 3.17–3.12 (m, 1H), 2.28 (s, 3H), 1.24 (d, J = 6.6 Hz, 6H). ^{13}C NMR (151 MHz, CDCl_3) δ 151.22, 134.11, 133.85, 126.97, 126.00, 117.78, 26.99, 22.61, 19.68. HRMS (ESI) m/z : calcd. for $\text{C}_{10}\text{H}_{12}\text{ClO}^-$, $[\text{M} - \text{H}]^-$, 183.0582. Found 183.0581.

4.1.3. 4-Bromo-2-isopropyl-5-methylphenol (**Thy2**)

To a solution of Thy (1 eq.) in MeOH: DCM (2:3 vol), was added tetrabutylammonium tribromide (1.0 eq.) at RT, and the mixture was stirred for 3 h. After the reaction completion, the solvent was concentrated under reduced pressure, the crude residue was purified by silica gel chromatography to afford **Thy2**. ^1H NMR (600 MHz, CDCl_3) δ 7.29 (s, 1H), 6.64 (s, 1H), 4.72 (s, 1H), 3.15–3.10 (m, 1H), 2.30 (s, 3H), 1.23 (d, J = 6.9 Hz, 6H). ^{13}C NMR (151 MHz, CDCl_3) δ 151.97, 136.01,

134.22, 130.19, 117.78, 115.74, 26.99, 22.63, 22.53. HRMS (ESI) m/z : calcd. for $\text{C}_{10}\text{H}_{12}\text{BrO}^-$, $[\text{M} - \text{H}]^-$, 227.0077. Found 227.0075.

4.1.4. General procedure for the preparation of **Thy3-Thy27**

To a solution of **Thy2** (1 eq.) and the respective boronic acid (2.5 eq.) in water:1,4-dioxane (4:1), was added sodium bicarbonate (10 eq.), degassed with nitrogen for 10 min, then added $\text{Pd}(\text{PPh}_3)_4$ (0.1 eq.), and the mixture was stirred at 80 °C overnight. After the reaction completion, the reaction mixture was diluted with water, and extracted with EtOAc twice, the organic layer was washed with brine, dried with anhydrous Na_2SO_4 , and concentrated under reduced pressure to get a crude compound. The crude product was purified by silica gel chromatography.

5-Isopropyl-2-methyl-[1,1'-biphenyl]-4-ol (Thy3**):** ^1H NMR (600 MHz, CDCl_3) δ 9.20 (s, 1H), 7.36 (t, J = 7.5 Hz, 2H), 7.25 (t, J = 5.2 Hz, 3H), 6.88 (s, 1H), 6.67 (s, 1H), 3.25–3.14 (m, 1H), 2.10 (s, 3H), 1.14 (d, J = 6.9 Hz, 6H). ^{13}C NMR (151 MHz, CDCl_3) δ 151.94, 142.10, 134.86, 133.92, 131.81, 129.59, 128.21, 128.14, 126.55, 117.07, 26.97, 22.83, 20.15. HRMS (ESI) m/z : calcd. for $\text{C}_{16}\text{H}_{17}\text{O}^-$, $[\text{M} - \text{H}]^-$, 225.1285. Found 225.1281.

2-Isopropyl-5-methyl-4-(pyridin-4-yl) phenol (Thy4**):** ^1H NMR (400 MHz, $\text{DMSO}-d_6$) δ 9.46 (s, 1H), 8.56 (d, J = 6.0 Hz, 1H), 7.32 (d, J = 6.1 Hz, 1H), 6.97 (s, 1H), 6.72 (s, 1H), 3.21–3.10 (m, 1H), 2.17 (s, 3H), 1.16 (d, J = 6.9 Hz, 6H). ^{13}C NMR (101 MHz, $\text{DMSO}-d_6$) δ 154.57, 149.33, 149.23, 132.73, 132.25, 129.27, 127.19, 124.27, 116.98, 116.93, 26.16, 22.47, 22.47, 19.79, 19.76. HRMS (ESI) m/z : calcd. for $\text{C}_{15}\text{H}_{16}\text{NO}^-$, $[\text{M} - \text{H}]^-$, 226.1237. Found 226.1234.

5-Isopropyl-2'-methoxy-2-methyl-[1,1'-biphenyl]-4-ol (Thy5**):** ^1H NMR (400 MHz, CDCl_3) δ 7.34 (m, 1H), 7.17 (dd, J = 7.3, 1.9 Hz, 1H), 7.05–6.95 (m, 3H), 6.66 (s, 1H), 4.82 (s, 1H), 3.79 (s, 3H), 3.25–3.14 (m, 1H), 2.08 (s, 3H), 1.27 (d, J = 6.8 Hz, 6H). ^{13}C NMR (101 MHz, CDCl_3) δ 156.92, 151.99, 135.38, 131.63, 131.42, 131.22, 130.94, 128.42, 120.52, 116.55, 116.51, 110.72, 55.53, 55.48, 26.94, 22.83, 19.63, 19.62. HRMS (ESI) m/z : calcd. for $\text{C}_{17}\text{H}_{19}\text{O}_2^-$, $[\text{M} - \text{H}]^-$, 255.1391. Found 255.1385.

5-Isopropyl-3'-methoxy-2-methyl-[1,1'-biphenyl]-4-ol (Thy6**):** ^1H NMR (400 MHz, CDCl_3) δ 7.25–7.22 (m, 2H), 7.05 (s, 1H), 6.97–6.93 (m, 2H), 6.66 (s, 1H), 4.83 (s, 1H), 3.86 (s, 3H), 3.25–3.15 (m, 1H), 2.20 (s, 3H), 1.27 (d, J = 6.8 Hz, 6H). ^{13}C NMR (101 MHz, CDCl_3) δ 158.34, 151.77, 134.54, 134.39, 134.00, 131.80, 130.58, 128.22, 117.04, 117.01, 113.55, 55.46, 26.94, 22.84, 20.22. HRMS (ESI) m/z : calcd. for $\text{C}_{17}\text{H}_{19}\text{O}_2^-$, $[\text{M} - \text{H}]^-$, 255.1391. Found 255.1387.

5-Isopropyl-4'-methoxy-2-methyl-[1,1'-biphenyl]-4-ol (Thy7**):** ^1H NMR (600 MHz, CDCl_3) δ 7.23 (d, J = 8.2 Hz, 2H), 7.04 (s, 1H), 6.94 (d, J = 8.1 Hz, 2H), 6.66 (s, 1H), 4.77 (s, 1H), 3.85 (s, 3H), 3.22–3.15 (m, 1H), 2.20 (s, 3H), 1.26 (d, J = 6.7 Hz, 6H). ^{13}C NMR (151 MHz, CDCl_3) δ 158.32, 151.81, 134.63, 134.38, 133.96, 131.88, 130.58, 128.21, 117.06, 113.59, 55.44, 26.95, 22.84, 20.18. HRMS (ESI) m/z : calcd. for $\text{C}_{17}\text{H}_{19}\text{O}_2^-$, $[\text{M} - \text{H}]^-$, 255.1391. Found 255.1387.

5'-Isopropyl-2'-methyl-[1,1'-biphenyl]-3,4'-diol (Thy8**):** ^1H NMR (400 MHz, CDCl_3) δ 7.24 (t, J = 8.4 Hz, 2H), 7.03 (s, 1H), 6.86 (d, J = 7.5 Hz, 1H), 6.79–6.74 (m, 2H), 6.64 (s, 1H), 3.20–3.12 (m, 1H), 2.19 (s, 3H), 1.24 (d, J = 6.8 Hz, 6H). ^{13}C NMR (101 MHz, CDCl_3) δ 155.35, 152.03, 143.84, 134.37, 133.84, 131.88, 129.30, 128.00, 122.20, 117.10, 116.60, 113.50, 29.84, 26.92, 22.83, 20.10. HRMS (ESI) m/z : calcd. for $\text{C}_{16}\text{H}_{17}\text{O}_2^-$, $[\text{M} - \text{H}]^-$, 241.1234. Found 241.1231.

5-Isopropyl-2-methyl-[1,1'-biphenyl]-4,4'-diol (Thy9**):** ^1H NMR (400 MHz, $\text{DMSO}-d_6$) δ 9.31 (s, 1H), 9.08 (s, 1H), 7.06–7.01 (m, 2H), 6.82 (s, 1H), 6.77–6.72 (m, 2H), 6.62 (s, 1H), 3.18–3.08 (m, 1H), 2.07 (s, 3H), 1.12 (d, J = 6.9 Hz, 6H). ^{13}C NMR (101 MHz, $\text{DMSO}-d_6$) δ 155.78, 153.04, 132.45, 132.35, 132.15, 131.53, 130.11, 127.19, 127.15, 116.55, 116.49, 114.80, 26.10, 22.62, 20.02, 19.98. HRMS (ESI) m/z : calcd. for $\text{C}_{16}\text{H}_{17}\text{O}_2^-$, $[\text{M} - \text{H}]^-$, 241.1234. Found 241.1232.

5-Isopropyl-2,2'-dimethyl-[1,1'-biphenyl]-4-ol (Thy10**):** ^1H NMR (400 MHz, CDCl_3) δ 7.34–7.24 (m, 3H), 7.21–7.17 (m, 1H), 7.00 (s, 1H), 6.72 (s, 1H), 5.06 (s, 1H), 3.33–3.22 (m, 1H), 2.14 (s, 3H), 2.04 (s, 3H),

1.31 (d, $J = 6.9$ Hz, 6H). ^{13}C NMR (101 MHz, CDCl_3) δ 151.67, 141.77, 136.45, 134.33, 134.23, 131.65, 130.01, 129.89, 127.56, 127.08, 125.57, 116.60, 116.57, 77.16, 26.86, 22.92, 22.85, 20.08, 19.49. HRMS (ESI) m/z : calcd. for $\text{C}_{17}\text{H}_{19}\text{O}^-$, $[\text{M} - \text{H}]^-$, 239.1441. Found 239.1438.

5-Isopropyl-2,3'-dimethyl-[1,1'-biphenyl]-4-ol (Thy11): ^1H NMR (400 MHz, CDCl_3) δ 7.39–7.34 (m, 1H), 7.24–7.18 (m, 3H), 7.14 (s, 1H), 6.72 (s, 1H), 5.12 (s, 1H), 3.34–3.24 (m, 1H), 2.48 (s, 3H), 2.28 (s, 3H), 1.35 (d, $J = 6.9$ Hz, 6H). ^{13}C NMR (101 MHz, CDCl_3) δ 151.85, 142.08, 137.69, 134.93, 133.83, 131.87, 130.31, 128.12, 128.00, 127.26, 126.65, 117.07, 117.05, 26.92, 22.84, 21.61, 20.13. HRMS (ESI) m/z : calcd. for $\text{C}_{17}\text{H}_{19}\text{O}^-$, $[\text{M} - \text{H}]^-$, 239.1441. Found 239.1438.

5-Isopropyl-2,4'-dimethyl-[1,1'-biphenyl]-4-ol (Thy12): ^1H NMR (400 MHz, CDCl_3) δ 7.27 (s, 4H), 7.12 (s, 1H), 6.70 (s, 1H), 4.98 (bs, 1H), 3.31–3.21 (m, 1H), 2.45 (s, 3H), 2.26 (s, 3H), 1.32 (d, $J = 6.9$ Hz, 6H). ^{13}C NMR (101 MHz, CDCl_3) δ 151.80, 139.16, 136.13, 134.74, 133.89, 131.87, 129.44, 128.85, 128.21, 117.08, 117.06, 26.92, 22.84, 21.27, 20.16. HRMS (ESI) m/z : calcd. for $\text{C}_{17}\text{H}_{19}\text{O}^-$, $[\text{M} - \text{H}]^-$, 239.1441. Found 239.1438.

2'-Fluoro-5-isopropyl-2-methyl-[1,1'-biphenyl]-4-ol (Thy13): ^1H NMR (400 MHz, CDCl_3) δ 7.39–7.28 (m, 2H), 7.26–7.13 (m, 2H), 7.10 (s, 1H), 6.73 (s, 1H), 5.30 (bs, 1H), 3.33–3.22 (m, 1H), 2.18 (s, 3H), 1.32 (d, $J = 7.0$ Hz, 6H). ^{13}C NMR (101 MHz, CDCl_3) δ 159.96 (d, $J = 245.2$ Hz), 152.54, 135.21, 132.06 (d, $J = 3.8$ Hz), 131.92, 129.41 (d, $J = 16.8$ Hz), 128.80 (d, $J = 8.0$ Hz), 128.41 (d, $J = 4.5$ Hz), 124.01 (d, $J = 3.6$ Hz), 116.84, 116.82, 115.55 (d, $J = 22.8$ Hz), 26.90, 22.78, 19.60, 19.56. HRMS (ESI) m/z : calcd. for $\text{C}_{16}\text{H}_{16}\text{FO}^-$, $[\text{M} - \text{H}]^-$, 243.1191. Found 243.1187.

3'-Fluoro-5-isopropyl-2-methyl-[1,1'-biphenyl]-4-ol (Thy14): ^1H NMR (400 MHz, CDCl_3) δ 7.38–7.30 (m, 1H), 7.08 (dd, $J = 7.8$, 2.8 Hz, 1H), 7.04–6.98 (m, 3H), 6.66 (s, 1H), 4.82 (bs, 1H), 3.25–3.14 (m, 1H), 2.19 (s, 3H), 1.26 (d, $J = 6.9$ Hz, 6H). ^{13}C NMR (101 MHz, CDCl_3) δ 162.64 (d, $J = 245.5$ Hz), 152.30, 133.85, 133.60 (d, $J = 1.9$ Hz), 132.02, 129.53 (d, $J = 8.5$ Hz), 128.04, 125.35 (d, $J = 2.8$ Hz), 117.19, 117.17, 116.51 (d, $J = 21.0$ Hz), 113.39 (d, $J = 21.0$ Hz), 26.98, 22.79, 20.07. HRMS (ESI) m/z : calcd. for $\text{C}_{16}\text{H}_{16}\text{FO}^-$, $[\text{M} - \text{H}]^-$, 243.1191. Found 243.1189.

4'-Fluoro-5-isopropyl-2-methyl-[1,1'-biphenyl]-4-ol (Thy15): ^1H NMR (400 MHz, CDCl_3) δ 7.33–7.26 (m, 2H), 7.16–7.10 (m, 2H), 7.08 (s, 1H), 6.70 (s, 1H), 5.07 (bs, 1H), 3.31–3.21 (m, 1H), 2.21 (s, 3H), 1.31 (d, $J = 7.0$ Hz, 6H). ^{13}C NMR (101 MHz, CDCl_3) δ 161.83 (d, $J = 245.0$ Hz), 152.04, 138.00 (d, $J = 3.4$ Hz), 133.92, 133.81, 132.02, 131.03 (d, $J = 8.0$ Hz), 128.14, 117.15, 117.12, 114.96 (d, $J = 21.1$ Hz), 26.94, 22.80, 20.08. HRMS (ESI) m/z : calcd. for $\text{C}_{16}\text{H}_{16}\text{FO}^-$, $[\text{M} - \text{H}]^-$, 243.1191. Found 243.1187.

2'-Chloro-5-isopropyl-2-methyl-[1,1'-biphenyl]-4-ol (Thy16): ^1H NMR (400 MHz, CDCl_3) δ 7.47–7.42 (m, 1H), 7.31–7.20 (m, 3H), 6.95 (s, 1H), 6.66 (s, 1H), 4.73 (s, 1H), 3.23–3.13 (m, 1H), 2.04 (s, 3H), 1.26–1.23 (m, 6H). ^{13}C NMR (101 MHz, CDCl_3) δ 152.32, 140.76, 134.79, 134.00, 132.22, 131.76, 131.63, 129.46, 128.43, 127.88, 126.61, 116.61, 26.94, 22.90, 22.69, 19.48. HRMS (ESI) m/z : calcd. for $\text{C}_{16}\text{H}_{16}\text{ClO}^-$, $[\text{M} - \text{H}]^-$, 259.0895. Found 259.0889.

3'-Chloro-5-isopropyl-2-methyl-[1,1'-biphenyl]-4-ol (Thy17): ^1H NMR (400 MHz, CDCl_3) δ 7.36–7.28 (m, 3H), 7.20 (dt, $J = 6.8$, 1.8 Hz, 1H), 7.04 (s, 1H), 6.68 (s, 1H), 4.95 (bs, 1H), 3.25–3.16 (m, 1H), 2.21 (s, 3H), 1.28 (d, $J = 6.9$ Hz, 6H). ^{13}C NMR (101 MHz, CDCl_3) δ 152.31, 143.92, 133.92, 133.85, 133.40, 132.06, 129.60, 129.36, 128.01, 127.82, 126.65, 117.17, 117.14, 26.95, 22.79, 20.07. HRMS (ESI) m/z : calcd. for $\text{C}_{16}\text{H}_{16}\text{ClO}^-$, $[\text{M} - \text{H}]^-$, 259.0895. Found 259.0892.

4'-Chloro-5-isopropyl-2-methyl-[1,1'-biphenyl]-4-ol (Thy18): ^1H NMR (400 MHz, CDCl_3) δ 8.10–8.05 (m 2H), 7.59–7.48 (m, 2H), 7.06 (s, 1H), 6.69 (s, 1H), 3.26–3.15 (m, 1H), 2.20 (s, 3H), 1.27 (d, $J = 7.0$ Hz, 6H). ^{13}C NMR (101 MHz, CDCl_3) δ 171.92, 152.36, 142.52, 135.00, 133.92, 133.54, 132.12, 131.24, 129.22, 128.40, 128.12, 117.24, 27.02, 22.80, 20.11. HRMS (ESI) m/z : calcd. for $\text{C}_{16}\text{H}_{16}\text{ClO}^-$, $[\text{M} - \text{H}]^-$, 259.0895. Found 259.0892.

4'-Hydroxy-5'-isopropyl-2'-methyl-[1,1'-biphenyl]-2-carboxylic acid (Thy19): ^1H NMR (400 MHz, $\text{DMSO}-d_6$) δ 12.35 (bs, 1H), 9.09 (s, 1H), 7.71 (d, $J = 7.7$ Hz, 1H), 7.47 (t, $J = 7.6$ Hz, 1H), 7.37 (t, $J = 7.6$ Hz, 1H), 7.16 (d, $J = 7.6$ Hz, 1H), 6.72 (s, 1H), 6.59 (s, 1H), 3.18–3.08 (m, 1H), 1.91 (s, 3H), 1.09 (d, $J = 6.8$ Hz, 6H). ^{13}C NMR (101 MHz, $\text{DMSO}-d_6$) δ 169.34, 153.31, 141.55, 132.95, 132.59, 131.80, 131.29, 130.80, 130.49, 128.89, 126.56, 116.02, 26.11, 22.59, 19.56. HRMS (ESI) m/z : calcd. for $\text{C}_{17}\text{H}_{17}\text{O}_3^-$, $[\text{M} - \text{H}]^-$, 269.1183. Found 269.1180.

4'-Hydroxy-5'-isopropyl-2'-methyl-[1,1'-biphenyl]-3-carboxylic acid (Thy20): ^1H NMR (600 MHz, CDCl_3) δ 8.06 (d, $J = 4.8$ Hz, 2H), 7.55 (d, $J = 7.6$ Hz, 1H), 7.52–7.48 (m, 1H), 7.05 (s, 1H), 6.69 (s, 1H), 3.24–3.17 (m, 1H), 2.20 (s, 3H), 1.27 (d, $J = 6.6$ Hz, 6H). ^{13}C NMR (151 MHz, CDCl_3) δ 172.27, 152.41, 142.57, 135.02, 133.90, 133.55, 132.22, 131.26, 129.29, 128.40, 128.12, 117.29, 27.02, 22.80, 20.08. HRMS (ESI) m/z : calcd. for $\text{C}_{17}\text{H}_{17}\text{O}_3^-$, $[\text{M} - \text{H}]^-$, 269.1183. Found 269.1178.

4'-Hydroxy-5'-isopropyl-2'-methyl-[1,1'-biphenyl]-4-carboxylic acid (Thy21): ^1H NMR (400 MHz, CDCl_3) δ 8.15 (d, $J = 8.1$ Hz, 2H), 7.43 (d, $J = 8.2$ Hz, 2H), 7.07 (s, 1H), 6.69 (s, 1H), 3.24–3.17 (m, 1H), 1.27 (d, $J = 6.9$ Hz, 6H). ^{13}C NMR (151 MHz, CDCl_3) δ 172.19, 152.63, 147.99, 133.84, 133.59, 132.31, 130.16, 129.77, 128.03, 127.41, 117.39, 77.16, 26.99, 22.79, 20.11. HRMS (ESI) m/z : calcd. for $\text{C}_{17}\text{H}_{17}\text{O}_3^-$, $[\text{M} - \text{H}]^-$, 269.1183. Found 269.1179.

4'-Hydroxy-5'-isopropyl-2'-methyl-[1,1'-biphenyl]-2-carbonitrile (Thy22): ^1H NMR (600 MHz, CDCl_3) δ 7.73 (d, $J = 7.7$ Hz, 1H), 7.61 (t, $J = 7.7$ Hz, 1H), 7.42 (t, $J = 7.7$ Hz, 1H), 7.38 (d, $J = 7.8$ Hz, 1H), 7.02 (s, 1H), 6.68 (s, 1H), 4.98 (s, 1H), 3.23–3.16 (m, 1H), 2.12 (s, 3H), 1.26 (d, $J = 6.8$ Hz, 6H). ^{13}C NMR (151 MHz, CDCl_3) δ 153.35, 146.36, 134.19, 132.96, 132.49, 132.19, 131.11, 130.52, 128.03, 127.25, 118.69, 117.17, 113.20, 26.90, 22.71, 19.58. HRMS (ESI) m/z : calcd. for $\text{C}_{17}\text{H}_{16}\text{NO}^-$, $[\text{M} - \text{H}]^-$, 250.1237. Found 250.1234.

4'-Hydroxy-5'-isopropyl-2'-methyl-[1,1'-biphenyl]-3-carbonitrile (Thy23): ^1H NMR (400 MHz, CDCl_3) δ 7.62–7.59 (m, 2H), 7.57–7.47 (m, 2H), 6.99 (s, 1H), 6.69 (s, 1H), 5.02 (bs, 1H), 3.26–3.16 (m, 1H), 2.18 (s, 3H), 1.26 (d, $J = 6.8$ Hz, 6H). ^{13}C NMR (101 MHz, CDCl_3) δ 152.81, 143.38, 134.13, 133.76, 133.07, 132.44, 132.33, 130.19, 129.01, 128.02, 119.15, 117.35, 112.27, 77.16, 26.96, 22.75, 20.01. HRMS (ESI) m/z : calcd. for $\text{C}_{17}\text{H}_{16}\text{NO}^-$, $[\text{M} - \text{H}]^-$, 250.1237. Found 250.1235.

4'-Hydroxy-5'-isopropyl-2'-methyl-[1,1'-biphenyl]-4-carbonitrile (Thy24): ^1H NMR (400 MHz, CDCl_3) δ 7.69 (d, $J = 8.2$ Hz, 2H), 7.42 (d, $J = 8.1$ Hz, 2H), 7.01 (s, 1H), 6.70 (s, 1H), 5.09 (bs, 1H), 3.27–3.17 (m, 1H), 2.20 (s, 3H), 1.26 (d, $J = 6.8$ Hz, 6H). ^{13}C NMR (151 MHz, CDCl_3) δ 153.05, 147.19, 133.64, 132.67, 132.55, 132.00, 130.33, 127.91, 119.24, 117.44, 110.03, 77.16, 26.93, 22.73, 20.01. HRMS (ESI) m/z : calcd. for $\text{C}_{17}\text{H}_{16}\text{NO}^-$, $[\text{M} - \text{H}]^-$, 250.1234.

5-Isopropyl-2-methyl-2'-(trifluoromethyl)-[1,1'-biphenyl]-4-ol (Thy25): ^1H NMR (600 MHz, CDCl_3) δ 7.74 (d, $J = 7.9$ Hz, 1H), 7.54 (t, $J = 7.6$ Hz, 1H), 7.44 (t, $J = 7.8$ Hz, 1H), 7.25 (s, 1H), 6.94 (s, 1H), 6.64 (s, 1H), 4.78 (bs, 1H), 3.22–3.15 (m, 1H), 1.95 (s, 3H), 1.22 (d, $J = 6.8$ Hz, 6H). ^{13}C NMR (151 MHz, CDCl_3) δ 154.77, 143.61, 137.03, 134.90, 134.15, 133.83, 133.44, 131.83 (q, $J = 29.2$ Hz), 130.49, 129.72, 128.60 (q, $J = 5.2$ Hz), 126.73 (q, $J = 273.9$ Hz), 118.86, 29.25, 25.40, 25.16, 22.22. ^{13}C NMR (151 MHz, CDCl_3) δ 152.24, 141.08, 134.50, 132.37, 131.62, 131.31, 130.91, 129.31 (q, $J = 29.2$ Hz), 127.98, 127.19, 126.08 (q, $J = 5.2$ Hz), 124.21 (q, $J = 273.9$ Hz), 116.33, 26.73, 22.88, 22.65, 19.70. HRMS (ESI) m/z : calcd. for $\text{C}_{17}\text{H}_{16}\text{F}_3\text{O}^-$, $[\text{M} - \text{H}]^-$, 293.1159. Found 293.1151.

5-Isopropyl-2-methyl-3'-(trifluoromethyl)-[1,1'-biphenyl]-4-ol (Thy26): ^1H NMR (400 MHz, CDCl_3) δ 7.58 (dd, $J = 6.6$, 1.8 Hz, 2H), 7.54–7.48 (m, 2H), 7.03 (s, 1H), 6.69 (s, 1H), 4.86 (bs, 1H), 3.26–3.16 (m, 1H), 2.19 (s, 3H), 1.27 (d, $J = 7.0$ Hz, 6H). ^{13}C NMR (151 MHz, CDCl_3) δ 155.05, 145.41, 136.45, 135.92, 135.47, 134.84, 133.10 (q, $J = 32.0$ Hz), 131.16, 130.65, 128.80 (q, $J = 3.5$ Hz), 126.95 (q, $J = 272.3$ Hz), 125.89 (q, $J = 3.5$ Hz), 119.86, 29.57, 25.36, 22.52. ^{13}C NMR (151 MHz, CDCl_3) δ 152.51, 142.87, 133.91, 133.39, 132.93, 132.30, 130.57 (q, $J = 32.0$ Hz), 128.62, 128.11, 126.28 (q, $J = 3.9$ Hz), 124.42 (q, $J =$

272.3 Hz), 123.36 (q, $J = 3.8$ Hz), 117.32, 27.04, 22.77, 20.00. HRMS (ESI) m/z : calcd. for $C_{17}H_{16}F_3 O^-$, [M – H][–], 293.1159. Found 293.1154.

5-Isopropyl-2-methyl-4’-(trifluoromethyl)-[1,1’-biphenyl]-4-ol (**Thy27**): ¹H NMR (400 MHz, CDCl₃) δ 7.66 (d, $J = 6.0$ Hz, 2H), 7.43 (d, $J = 8.3$ Hz, 2H), 7.04 (d, $J = 3.3$ Hz, 1H), 6.69 (d, $J = 2.2$ Hz, 1H), 4.85 (bs, 1H), 3.26–3.15 (m, 1H), 2.20 (s, 3H), 1.28–1.25 (m, 6H). ¹³C NMR (151 MHz, CDCl₃) δ 152.55, 145.84, 133.87, 133.43, 132.25, 129.90, 128.76 (q, $J = 32.2$ Hz), 128.08, 125.11 (q, $J = 3.8$ Hz), 124.54 (q, $J = 271.6$ Hz), 117.32, 27.00, 22.77, 20.03. HRMS (ESI) m/z : calcd. for $C_{17}H_{16}F_3 O^-$, [M – H][–], 293.1159. Found 293.1154.

4.1.5. General procedure for the preparation of intermediates **2a–2i**

The solution of the respective bromoalkylacid (1 eq.) and triphenylphosphine (1 eq.) in acetonitrile (5 mL) was refluxed for 72 h. After the reaction completion, the solvent was removed and the crude product was purified by silica gel chromatography to afford intermediate **2a–2i**.

(2-Carboxyethyl)triphenylphosphonium bromide (**2a**): ¹H NMR (400 MHz, CDCl₃) δ 7.81–7.60 (m, 15H), 3.76–3.65 (m, 2H), 2.96–2.85 (m, 2H). ¹³C NMR (101 MHz, DMSO-d₆) δ 171.42, 171.28, 135.41, 135.39, 133.73, 133.63, 130.76, 130.64, 117.90, 117.04, 28.02, 19.15, 18.61.

(3-Carboxypropyl)triphenylphosphonium bromide (**2b**): ¹H NMR (400 MHz, DMSO-d₆) δ 7.92–7.67 (m, 15H), 3.74–3.68 (m, 2H), 2.52 (t, $J = 6.9$ Hz, 2H), 1.73–1.68 (m, 2H). ¹³C NMR (101 MHz, DMSO-d₆) δ 173.32, 134.93, 133.62, 133.52, 130.31, 130.19, 118.78, 117.93, 33.72, 33.54, 20.12, 19.61, 17.78.

(4-Carboxybutyl)triphenylphosphonium bromide (**2c**): ¹H NMR (400 MHz, CDCl₃) δ 7.86–7.57 (m, 15H), 3.64–3.57 (m, 2H), 2.58 (t, $J = 6.8$ Hz, 2H), 1.94–1.87 (m, 2H), 1.74–1.65 (m, 2H). ¹³C NMR (101 MHz, CDCl₃) δ 175.06, 135.28, 135.25, 133.77, 133.67, 130.76, 130.64, 118.52, 117.66, 33.87, 25.73, 25.56, 22.71, 22.20, 21.67.

(5-Carboxypentyl)triphenylphosphonium bromide (**2d**): ¹H NMR (400 MHz, CDCl₃) δ 7.96–7.49 (m, 15H), 3.55–3.48 (m, 2H), 2.26 (t, $J = 6.5$ Hz, 2H), 1.61–1.54 (m, 6H). ¹³C NMR (101 MHz, CDCl₃) δ 175.91, 135.19, 135.16, 133.66, 133.56, 130.68, 130.55, 118.52, 117.66, 34.17, 29.64, 29.48, 24.05, 22.76, 22.25, 22.01, 21.97.

(6-Carboxyhexyl)triphenylphosphonium bromide (**2e**): ¹H NMR (400 MHz, CDCl₃) δ 7.89–7.59 (m, 15H), 3.63–3.51 (m, 2H), 2.36 (t, $J = 7.1$ Hz, 2H), 1.69–1.57 (m, 4H), 1.54–1.50 (m, 2H), 1.36–1.29 (m, 2H). ¹³C NMR (101 MHz, CDCl₃) δ 176.44, 135.24, 133.78, 133.68, 130.75, 130.62, 118.70, 117.84, 34.47, 29.60, 29.45, 27.91, 24.27, 22.85, 22.35, 22.18.

(7-Carboxyheptyl)triphenylphosphonium bromide (**2f**): ¹H NMR (400 MHz, CDCl₃) δ 7.71 (m, 15H), 3.56–3.46 (m, 2H), 2.28 (t, $J = 7.3$ Hz, 2H), 1.52 (m, 6H), 1.34–1.11 (m, 4H). ¹³C NMR (101 MHz, CDCl₃) δ 176.70, 135.19, 135.17, 133.66, 133.56, 130.68, 130.56, 118.61, 117.75, 34.40, 30.02, 29.86, 28.25, 28.15, 24.52, 22.84, 22.34.

(8-Carboxyoctyl)triphenylphosphonium bromide (**2g**): ¹H NMR (400 MHz, CDCl₃) δ 7.91–7.45 (m, 15H), 3.55–3.48 (m, 2H), 2.24 (t, $J = 7.4$ Hz, 2H), 1.67–1.39 (m, 6H), 1.27–1.09 (m, 6H). ¹³C NMR (101 MHz, CDCl₃) δ 176.92, 135.18, 135.16, 133.64, 133.54, 130.66, 130.54, 118.61, 117.76, 34.44, 30.18, 30.02, 28.51, 24.60, 22.89, 22.47, 22.42.

(9-Carboxynonyl)triphenylphosphonium bromide (**2h**): ¹H NMR (400 MHz, CDCl₃) δ 7.92–7.59 (m, 15H), 3.67–3.61 (m, 2H), 2.36 (t, $J = 7.2$ Hz, 2H), 1.66–1.43 (m, 6H), 1.27–1.17 (m, 8H). ¹³C NMR (101 MHz, CDCl₃) δ 177.12, 135.15, 133.59, 133.49, 130.63, 130.51, 118.54, 117.68, 34.38, 30.25, 30.09, 28.63, 24.61, 22.81, 22.39.

(10-Carboxydecyl)triphenylphosphonium bromide (**2i**): ¹H NMR (400 MHz, CDCl₃) δ 7.89–7.52 (m, 15H), 3.58–3.49 (m, 2H), 2.28 (t, $J = 7.4$ Hz, 2H), 1.62–1.45 (m, 6H), 1.24–1.06 (m, 10H). ¹³C NMR (101 MHz, CDCl₃) δ 177.33, 135.17, 135.14, 133.65, 133.55, 130.65, 130.53, 118.65, 117.80, 34.44, 30.39, 30.24, 28.99, 28.86, 28.77, 24.73, 22.93, 22.55, 22.50, 22.43.

4.1.6 General procedure for the preparation of **Thy3a–Thy3i**.

To a solution of intermediates **2a–2i** (1 eq.) in DCM, added DCC and DMAP, and **Thy3**, then the mixture was stirred overnight at RT. After the

reaction completion, the solvent was removed and the crude product was purified by silica gel chromatography to afford **Thy3a–Thy3i**.

(3-((5-Isopropyl-2-methyl-[1,1’-biphenyl]-4-yl)oxy)-3-oxopropyl)triphenylphosphonium bromide (**Thy3a**): ¹H NMR (600 MHz, DMSO-d₆) δ 7.92 (t, $J = 7.3$ Hz, 3H), 7.88–7.85 (m, 6H), 7.81–7.77 (m, 6H), 7.43 (t, $J = 7.5$ Hz, 2H), 7.38–7.30 (m, 3H), 7.11 (s, 1H), 6.86 (s, 1H), 4.00–3.95 (m, 2H), 3.09–3.04 (m, 2H), 2.91–2.86 (m, 1H), 2.15 (s, 3H), 1.09 (d, $J = 6.9$ Hz, 6H). ¹³C NMR (151 MHz, DMSO-d₆) δ 169.63, 169.51, 146.60, 140.61, 139.52, 137.16, 135.12, 135.10, 133.84, 133.77, 133.38, 130.36, 130.28, 129.01, 128.26, 127.70, 127.02, 123.64, 118.29, 117.71, 26.75, 26.26, 22.93, 19.66, 16.98, 16.62. HRMS (ESI) m/z : calcd for C₃₇H₃₆O₂P, [M – Br]⁺, 543.2447. Found 543.2465.

(4-((5-Isopropyl-2-methyl-[1,1’-biphenyl]-4-yl)oxy)-4-oxobutyl)triphenylphosphonium bromide (**Thy3b**): ¹H NMR (400 MHz, DMSO-d₆) δ 7.91–7.74 (m, 15H), 7.41 (t, $J = 7.3$ Hz, 2H), 7.35–7.30 (m, 3H), 7.09 (s, 1H), 6.98 (s, 1H), 3.71–3.62 (m, 2H), 2.88 (t, $J = 7.2$ Hz, 2H), 2.14 (s, 3H), 1.92–1.83 (m, 2H), 1.07 (d, $J = 6.9$ Hz, 6H). ¹³C NMR (101 MHz, DMSO-d₆) δ 170.95, 146.69, 140.71, 139.34, 137.03, 135.09, 133.68, 133.58, 133.36, 130.43, 130.31, 129.05, 128.30, 127.68, 127.04, 124.01, 118.71, 117.85, 33.68, 33.49, 26.61, 22.82, 20.07, 19.72, 19.56, 18.71, 17.79. HRMS (ESI) m/z : calcd for C₃₈H₃₈O₂P, [M – Br]⁺, 557.2604. Found 557.2623.

(5-((5-Isopropyl-2-methyl-[1,1’-biphenyl]-4-yl)oxy)-5-oxopentyl)triphenylphosphonium bromide (**Thy3c**): ¹H NMR (600 MHz, DMSO-d₆) δ 7.89 (t, $J = 7.4$ Hz, 3H), 7.84–7.73 (m, 12H), 7.43 (t, $J = 7.5$ Hz, 2H), 7.36–7.32 (m, 3H), 7.10 (s, 1H), 6.85 (s, 1H), 3.69–3.64 (m, 2H), 2.88–2.83 (m, 1H), 2.72 (t, $J = 7.4$ Hz, 2H), 2.15 (s, 3H), 1.88–1.83 (m, 2H), 1.70–1.63 (m, 2H), 1.07 (d, $J = 6.9$ Hz, 6H). ¹³C NMR (151 MHz, DMSO-d₆) δ 171.73, 146.75, 140.71, 139.28, 137.14, 134.95, 133.62, 133.55, 133.37, 130.32, 130.24, 129.02, 128.26, 127.66, 126.99, 123.85, 118.77, 118.20, 32.49, 26.58, 25.26, 25.14, 22.81, 21.25, 21.23, 20.20, 19.86, 19.67. HRMS (ESI) m/z : calcd for C₃₉H₄₀O₂P, [M – Br]⁺, 571.2760. Found 571.2771.

(6-((5-Isopropyl-2-methyl-[1,1’-biphenyl]-4-yl)oxy)-6-oxohexyl)triphenylphosphonium bromide (**Thy3d**): ¹H NMR (600 MHz, DMSO-d₆) δ 7.89 (t, $J = 7.3$ Hz, 3H), 7.83–7.73 (m, 12H), 7.43 (t, $J = 7.5$ Hz, 2H), 7.36–7.32 (m, 3H), 7.11 (s, 1H), 6.90 (s, 1H), 3.62–3.57 (m, 2H), 2.91–2.87 (m, 1H), 2.59 (t, $J = 7.3$ Hz, 2H), 2.15 (s, 3H), 1.71–1.66 (m, 4H), 1.62–1.54 (m, 4H), 1.11 (d, $J = 6.9$ Hz, 6H). ¹³C NMR (151 MHz, DMSO-d₆) δ 171.88, 146.82, 140.74, 139.24, 137.17, 134.91, 133.65, 133.59, 133.37, 130.29, 130.21, 129.03, 128.27, 127.65, 126.99, 123.92, 118.85, 118.28, 33.09, 29.32, 29.20, 26.62, 23.64, 22.83, 21.59, 21.56, 20.38, 20.04, 19.68. HRMS (ESI) m/z : calcd for C₄₀H₄₂O₂P, [M – Br]⁺, 585.2917. Found 585.2930.

(7-((5-Isopropyl-2-methyl-[1,1’-biphenyl]-4-yl)oxy)-7-oxoheptyl)triphenylphosphonium bromide (**Thy3e**): ¹H NMR (600 MHz, DMSO-d₆) δ 7.88 (t, $J = 7.3$ Hz, 3H), 7.82–7.73 (m, 12H), 7.43 (t, $J = 7.5$ Hz, 2H), 7.36–7.32 (m, 3H), 7.11 (s, 1H), 6.91 (s, 1H), 3.61–3.56 (m, 2H), 2.92–2.85 (m, 1H), 2.58 (t, $J = 7.4$ Hz, 2H), 2.15 (s, 3H), 1.63–1.50 (m, 6H), 1.36–1.41 (m, 2H), 1.10 (d, $J = 6.9$ Hz, 6H). ¹³C NMR (151 MHz, DMSO-d₆) δ 171.96, 146.83, 140.74, 139.22, 137.12, 134.89, 133.62, 133.55, 133.36, 130.28, 130.20, 129.02, 128.25, 127.62, 126.97, 123.95, 118.85, 118.28, 33.33, 29.53, 29.42, 27.58, 26.61, 24.81, 24.13, 22.79, 21.68, 21.65, 20.37, 20.04, 19.65. HRMS (ESI) m/z : calcd for C₄₁H₄₄O₂P, [M – Br]⁺, 599.3073. Found 599.3092.

(8-((5-Isopropyl-2-methyl-[1,1’-biphenyl]-4-yl)oxy)-8-oxooctyl)triphenylphosphonium bromide (**Thy3f**): ¹H NMR (600 MHz, DMSO-d₆) δ 7.88 (t, $J = 7.2$ Hz, 3H), 7.82–7.72 (m, 12H), 7.43 (t, $J = 7.5$ Hz, 2H), 7.39–7.30 (m, 3H), 7.11 (s, 1H), 6.91 (s, 1H), 3.59–3.53 (m, 2H), 2.92–2.88 (m, 1H), 2.59 (t, $J = 7.3$ Hz, 2H), 2.15 (s, 3H), 1.65–1.60 (m, 2H), 1.56–1.50 (m, 2H), 1.49–1.44 (m, 2H), 1.35–1.28 (m, 4H), 1.11 (d, $J = 6.9$ Hz, 6H). ¹³C NMR (151 MHz, DMSO-d₆) δ 172.06, 146.85, 140.75, 139.23, 137.16, 134.89, 133.61, 133.55, 133.38, 130.29, 130.21, 129.02, 128.27, 127.64, 126.98, 123.94, 118.88, 118.31, 33.36, 29.76, 29.65, 28.14, 27.81, 26.61, 24.31, 22.82, 21.78, 21.75, 20.35,

20.02, 19.66. HRMS (ESI) m/z : calcd for $C_{42}H_{46}O_2P$, [M – Br]⁺, 613.3230. Found 613.3246.

(9-((5-Isopropyl-2-methyl-[1,1'-biphenyl]-4-yl)oxy)-9-oxononyl)triphenylphosphonium bromide (**Thy3g**): ¹H NMR (600 MHz, DMSO-*d*₆) δ 7.88 (t, *J* = 7.3 Hz, 3H), 7.81–7.73 (m, 12H), 7.43 (t, *J* = 7.5 Hz, 2H), 7.38–7.30 (m, 3H), 7.11 (s, 1H), 6.92 (s, 1H), 3.59–3.52 (m, 2H), 2.93–2.89 (m, 1H), 2.58 (t, *J* = 7.3 Hz, 2H), 2.15 (s, 3H), 1.65–1.60 (m, 2H), 1.55–1.49 (m, 2H), 1.48–1.43 (m, 2H), 1.35–1.20 (m, 6H), 1.11 (d, *J* = 7.0 Hz, 6H). ¹³C NMR (151 MHz, DMSO-*d*₆) δ 172.02, 146.84, 140.74, 139.20, 137.13, 134.85, 133.60, 133.54, 133.36, 130.26, 130.18, 129.00, 128.24, 127.61, 126.95, 123.93, 118.87, 118.30, 33.43, 29.82, 29.71, 28.36, 28.29, 27.99, 26.60, 24.37, 22.80, 21.77, 21.74, 20.35, 20.02, 19.64. HRMS (ESI) m/z : calcd for $C_{43}H_{48}O_2P$, [M – Br]⁺, 627.3386. Found 627.3398.

(10-((5-Isopropyl-2-methyl-[1,1'-biphenyl]-4-yl)oxy)-10-oxodecyl)triphenylphosphonium bromide (**Thy3h**): ¹H NMR (400 MHz, CDCl₃) δ 7.76–7.57 (m, 15H), 7.32 (t, *J* = 7.3 Hz, 2H), 7.27–7.19 (m, 3H), 7.06 (s, 1H), 6.80 (s, 1H), 3.52–3.46 (m, 2H), 2.94–2.87 (m, 1H), 2.50 (t, *J* = 7.5 Hz, 2H), 2.12 (s, 3H), 1.62–1.70 (m, 2H), 1.56–1.50 (m, 4H), 1.32–1.28 (m, 2H), 1.27–1.17 (m, 6H), 1.10 (d, *J* = 7.0 Hz, 6H). ¹³C NMR (101 MHz, CDCl₃) δ 172.50, 146.86, 141.32, 139.59, 137.11, 134.95, 134.93, 133.65, 133.37, 133.27, 130.43, 130.31, 129.04, 127.88, 126.63, 123.49, 118.42, 117.56, 34.14, 33.58, 30.32, 30.16, 28.91, 28.83, 26.94, 24.99, 24.76, 22.87, 22.42, 22.38, 21.93, 19.88. HRMS (ESI) m/z : calcd for $C_{44}H_{50}O_2P$, [M – Br]⁺, 641.35. Found 641.36.

(11-((5-Isopropyl-2-methyl-[1,1'-biphenyl]-4-yl)oxy)-11-oxoundecyl)triphenylphosphonium bromide (**Thy3i**): ¹H NMR (600 MHz, DMSO-*d*₆) δ 7.87 (t, *J* = 7.2 Hz, 3H), 7.82–7.71 (m, 12H), 7.43 (t, *J* = 7.5 Hz, 2H), 7.36–7.32 (m, 3H), 7.11 (s, 1H), 6.92 (s, 1H), 3.56–3.52 (m, 2H), 2.94–2.89 (m, 1H), 2.59 (t, *J* = 7.3 Hz, 2H), 2.15 (s, 3H), 1.66–1.61 (m, 2H), 1.54–1.48 (m, 2H), 1.46–1.41 (m, 2H), 1.36–1.31 (m, 2H), 1.28–1.25 (m, 4H), 1.20–1.18 (m, 4H), 1.12 (d, *J* = 6.8 Hz, 6H). ¹³C NMR (151 MHz, DMSO-*d*₆) δ 172.06, 146.85, 140.75, 139.20, 137.14, 134.87, 134.85, 133.60, 133.53, 133.37, 130.26, 130.18, 129.01, 128.25, 127.62, 126.96, 123.93, 118.86, 118.30, 33.44, 29.87, 29.77, 28.74, 28.64, 28.60, 28.40, 28.11, 26.59, 24.43, 22.81, 21.77, 21.74, 20.34, 20.01, 19.64. HRMS (ESI) m/z : calcd for $C_{45}H_{52}O_2P$, [M – Br]⁺, 655.3699. Found 655.3709.

4.2. Antimicrobial activity

The minimum inhibitory concentration (MIC) of the compounds was tested by the Clinical and Laboratory Standards Institute (CLSI) broth dilution procedure with minor modifications. Two Gram-positive bacteria (*S. aureus* and MRSA) and four Gram-negative bacteria (*E. coli*, *A. baumannii*, *P. aeruginosa*, and *K. pneumoniae*) were selected as the tested bacteria. Each bacterial suspension was adjusted to a concentration of 1×10^6 CFU/mL. All compounds were thoroughly dried before weighing. Initially, the compounds were dissolved in dimethyl sulfoxide (DMSO) to prepare the stock solutions. The tested compounds and ciprofloxacin were then prepared in liquid Luria–Bertan media. The concentration of Thymol was 512, 256, 128, 64, 32, 16, 8, 4, 2, 1 and 0.5 µg/mL. Their MICs of the preferred compounds **Thy1-27**, **Thy3a-3i**, and ciprofloxacin were also tested at concentrations of 64, 32, 16, 8, 4, 2, 1, 0.5, 0.25, 0.125, and 0.0625 µg/mL. After incubation at 37 °C for 18 h, the inhibition of bacterial growth in each well was determined by measuring absorbance at 595 nm with a microplate reader. The MIC of the compounds was defined as the lowest concentration that completely inhibited bacterial growth.

4.3. Cell toxicity

To determine the cytotoxicity of the compounds, we used the MTT dye reduction assay against the L02 cell. In brief, 1×10^5 cells in a 96-well plate were cultured overnight in DMEM and at 37 °C with 5% CO₂. The cells were washed twice with phosphate-buffered saline (PBS)

and fresh media was added. The compounds were serially diluted by halving concentrations in media and the cells were incubated for 72 h. Then, MTT solution (5 mg/mL) was added to the cells for 4 h. After incubation, the precipitated MTT formazan crystal was dissolved by DMSO. Absorbance at 595 nm was measured using a microplate reader.

4.4. Time kill kinetics

The *in vitro* time-kill kinetics of **Thy3d** and ciprofloxacin were performed against MRSA 3390. The bacteria were incubated on LB at 37 °C for 8 h, and then the inoculum was adjusted to approximately 10^6 CFU/mL. The bacterial suspension was incubated with samples at different concentrations (1, 2, 4, and 8 × MIC) at 37 °C. The aliquots were then removed from the mixtures at different time points (0, 1, 4, 6, and 24 h), and were serially diluted 10-fold in PBS (pH = 7.2) and plated with TSA medium. The plates were incubated at 37 °C for 24 h. The bactericidal efficacy of the compounds was evaluated by counting the bacterial colonies grown on the plates.

4.5. Drug resistance study

MRSA 3390 was employed to assess the development of resistance by the serial passaging method, as previously described [36]. The initial MICs for the compounds against MRSA 3390 were obtained according to the above method. Bacteria harvested from 96-well plates of 1/2 MIC levels, diluted in MHB to a concentration of 1×10^6 CFU/mL and then subjected to MIC determination. The experiment was repeated every day for 40 days.

4.6. MRSA persister cells eradicating assay

As has been previously demonstrated, stationary-phase cells of *S. aureus* can be used to model persister cells [37,38]. Briefly, a single clone of MRSA 3390 was inoculated into a TSB medium and cultivated until the stationary period. Then the culture was treated with ciprofloxacin (final concentration 40 µg/mL, 20 × MIC) for 6 h. The bacteria cells were collected by centrifugation (8000 rpm, 5 min, 4 °C) and washed with sterile PBS. Re-suspend the bacteria in sterile PBS to a density of OD₆₀₀ = 0.5. The bacteria re-suspension was treated with different concentrations of **Thy3d** (1, 2, 4, and 8 × MIC). Subsequently, 10 µL of the bacterial solution was taken at set time points (0, 1, 3, 5, and 7 h) and applied to the LB agar plate after series dilution. The number of colonies was counted after 24 h of culture at 37 °C. Bacteria re-suspension containing 1% DMSO was used as a negative control. Make three duplicate wells for each concentration of the drug, two plates in parallel for each dilution.

4.7. DNA leakage

The membrane permeability was performed by estimating the amounts of nucleic acids released as previously described with brief modification [39]. A single colony of MRSA 3390 was cultured in 20 mL TSB overnight at 37 °C. The culture was centrifuged at 8000 rpm for 5 min, then the supernatant was discarded and the bacterial pellet was washed with PBS. The bacteria were then re-suspended in PBS. The bacterial suspension was treated with different concentrations (1, 2, 4, and 8 × MIC) of **Thy3d**. The treatment of bacteria re-suspension containing 1% DMSO was used as a negative control. 1 mL sample was taken from cultures at different points (0, 1, 2, 4, and 6 h) and immediately sieved with 0.22 µm syringe filters to remove the bacterial cells. The released amount of DNA in the filtrate was measured at 260 nm with a micro-spectrophotometer.

The persisters were obtained according to method 4.6, and the DNA leakage of the persister was tested as described above.

4.8. SYTOX green assay

MRSA 3390 was incubated at 37 °C overnight. The culture was centrifuged at 8000 rpm for 5 min, then the supernatant was discarded and the bacterial pellet was washed with PBS to prepare bacterial suspension (2×10^7 CFU/mL). SYTOX™ Green was added to the bacterial suspension with a final concentration of 5 µM and kept in the dark for 20 min [40]. After the fluorescence signal had stabilized, the different concentrations (1, 2, 4, and $8 \times$ MIC) of compound **Thy3d** (final DMSO concentration of 0.5%) were added to the mixture, and the fluorescence intensity changes were monitored and recorded every 5 min, for a total of 120 min. The treatment of bacteria re-suspension containing 0.5% DMSO was used as a negative control, and the treatment of 1% Triton X-100 was used as a positive control. The effects of the **Thy3d** on the membrane permeability of normal bacteria were detected.

The persisters were obtained according to method 4.6, and the membrane permeability of the persister was tested as described above.

4.9. Membrane depolarization assay

MRSA 3390 was incubated in LB at 37 °C overnight. The culture was centrifuged at 8000 rpm for 5 min, then the supernatant was discarded and the bacterial pellet was washed 3 times with assay buffer (5 mM HEPES, 20 mM glucose, 100 mM KCl, pH 7.4), and finally resuspended in assay buffer, adjusting the OD₆₀₀ to 0.1. DiSC₃(5) (3,3'-dipropylthiocarbocyanine) dye was added to the cells at a final concentration of 3 µM [41]. The above bacteria suspension with DiSC₃(5) was added to each well of a 96-well black microplate and incubated at 37 °C until a stable fluorescence was observed. **Thy3d** was added into the wells at different concentrations (1, 2, 4, and $8 \times$ MIC). Plates were immediately read on an Envision at $\lambda_{\text{ex}} = 622$ nm/ $\lambda_{\text{em}} = 670$ nm (reading every 2 min) until the maximal intensity was achieved. The effects of the **Thy3d** on the membrane depolarization of normal bacteria were detected.

The persisters were obtained according to method 4.6, and the membrane depolarization of the persister was tested as described above.

4.10. SEM assay

A standard procedure was followed for SEM analysis [42]. MRSA 3390 was incubated to the logarithmic growth phase, then suspended in PBS buffer (pH 7.2) and adjusted to approximately 5×10^7 CFU/mL. The bacterial suspension was mixed with $4 \times$ MIC of **Thy3d** and incubated at 37 °C for 1 h. The PBS-treated group was used as a negative control. All samples were centrifuged at 5000 g for 5 min, washed, and resuspended in PBS. Bacterial cells were fixed with 2.5% glutaraldehyde and then incubated at 37 °C on a glass slide for 20 min. Samples were dehydrated by passing through gradient ethanol (10%, 30%, 50%, 70%, 90%, and 100%) for 5 min at each concentration. Slides were then dried with an automatic critical point drying instrument (Leica EM CPD300), and a small amount of gold was sputtered onto the samples using a sputter coater system. Morphology images were collected using a scanning electron microscope (Regulus 8100, Hitachi, Japan).

4.11. Molecular dynamics simulations

Atomistic molecular dynamics (MD) simulations were carried out to study the mode of interactions of **Thy3d** with a model bacterial membrane constructed out of 96 zwitterionic lipids POPE and 32 anionic lipids POPG and with the mammalian membrane was modelled using 96 zwitterionic lipids POPC and 32 cholesterol [43]. These models can capture the main structural features of bacterial membrane and has been widely used in previous studies [44–47].

To understand the membrane affinity of **Thy3d**, the free energy of adsorption of **Thy3d** on bacterial and mammalian membranes was carried out using umbrella sampling [48]. The distance between the center of mass of the **Thy3d** and the bilayer center was chosen as the

reaction coordinate. In each umbrella sampling, a total of 14 window simulations spanning the distance from 0 nm to 4 nm were carried out. Each window simulation was run for 400 ns, the free energy profile was constructed using the weighted histogram analysis method (WHAM) [49].

CHARMM36 m force field was used to model both the **Thy3d** and the membranes, and water molecules were modeling using CHARMM modified TIP3P model [50]. The topology of the peptide and lipids was generated using CHARMM-GUI [51]. In each simulation, the LJ interactions were calculated using a cutoff of 1.2 nm, with a force switch between 1.0 nm and 1.2 nm. The short-range electrostatic interactions were calculated with a cutoff of 1.2 nm while the long-range electrostatic interactions were computed using PME [52]. During the MD simulations, the covalent bonds involving hydrogen atoms were constrained using the LINCS algorithm, enabling a time step of 2 fs to be used. The simulations were run in an NPT ensemble, with temperature maintained at 300 K using the Nose-Hoover method and pressure maintained using the Parrinello-Rahman method with semi-isotropic pressure coupling. All simulations were carried out using GROMACS 2021.

4.12. Bilayer experiment and electrical recording

The bilayer experiments were performed according to the method described by Zhou with minor modifications [31]. Briefly, this experiment was performed in a planar bilayer chamber, which was separated into two compartments by a Teflon film, and the lipid bilayer was formed at a 156-µm-diameter aperture of the Teflon film using DPhPC according to the Montal–Mueller method [53]. All the experiments were carried out in the chamber with 2 mL of buffer solutions added in each compartment containing 1 M KCl, 10 mM Tris, and 1 mM EDTA (pH 7.6). The higher ion concentration than the one (0.15 M) used in the simulation can enhance the ionic current through the pore [54] achieving improved signal-to-noise ratios and meanwhile can screen charges of membrane/**Thy3d** at pH 7.6. **Thy3d** were added to the grounded cis compartment. An Axopatch 200B amplifier (Molecular Devices, Sunnyvale, CA) was used to record the ionic currents that were low-pass filtered with a built-in four-pole Bessel filter at 2 kHz and sampled at 50 kHz by a computer equipped with a Digidata 1440A converter (Molecular Devices).

4.13. Mouse skin infection model

Six-week-old adult female Balb/C mice were randomly divided into three groups with six mice in each group, and rendered neutropenic by injecting two doses of cyclophosphamide intraperitoneally 4 days (150 mg/kg) and 1 day (100 mg/kg) before experimental infection. *S. aureus* Xen29 bioluminescent bacteria were cultured under standard conditions [55]. On Day -1, the fur on the right leg of each of the mice was removed by shaving and application of chemical depilatories. On Day 0, approximately 1×10^9 CFU of bacteria in 100 µL were inoculated by subcutaneous injection in the right thigh of each mouse. A saline solution containing 5% DMSO was used to dissolve the drug. The success of modeling was observed by bioluminescent *in vivo* imaging 12 h after infection, and uninfected mice were excluded. **Thy3d** (8 mg/kg, 100 µL), vancomycin (8 mg/kg, 100 µL), or saline (100 µL) was injected into the mice by subcutaneous injection 16, 24, 36, 48, 60, and 72 h post-infection. The skin wound of the mice was monitored daily, and the weight of the mice was recorded every day.

Bioluminescent *in vivo* imaging was performed at 12, 24, 36, 60, and 84 h post-infection. On Day 4, 84 h after the infection, animals were sacrificed. Samples of skin from each animal were homogenized and plated on nutrient agar to determine the CFUs per animal. Animals were imaged using a Lumina II system (PerkinElmer), and bioluminescence (photons per second) was determined.

4.14. Statistical analysis

The statistical tests and several biological replicates and/or experiments were stated in the legend of the figure, with significance set at $p < 0.05$. All statistical data were analyzed by GraphPad Prism 8.0 statistical software.

CRediT authorship contribution statement

Ziyi Tang: Writing – review & editing, Writing – original draft, Project administration, Methodology, Funding acquisition, Data curation, Conceptualization. **Jizhou Feng:** Project administration, Methodology. **Mahesh Challa:** Data curation. **Sankara Rao Rowthu:** Software. **Shuxin Xiong:** Investigation. **Cheng Zou:** Formal analysis. **Jianguo Li:** Methodology. **Chandra Shekhar Verma:** Methodology. **Haibo Peng:** Conceptualization, Writing – original draft. **Xiaoli He:** Validation. **Chao Huang:** Resources, Visualization. **Yun He:** Conceptualization, Validation.

Declaration of competing interest

The authors declare that they have no known competing financial interests or personal relationships that could have appeared to influence the work reported in this paper.

Data availability

Data will be made available on request.

Acknowledgments

This work was supported by the National Natural Science Foundation of China (Grant No. 22071012), Chongqing Postdoctoral Science Foundation (Grant No. cstc2021jcyj-bshX0081). J.L. thanks the support from A*STAR Career Development Award grant (CDA, Grant No. 202D8155). The authors also thank the NSCC and ASTAR ACRC for providing the computational resources to perform simulations.

Appendix A. Supplementary data

Supplementary data to this article can be found online at <https://doi.org/10.1016/j.ejmech.2024.116381>.

References

- [1] J. Sunuwar, R.K. Azad, A machine learning framework to predict antibiotic resistance traits and yet unknown genes underlying resistance to specific antibiotics in bacterial strains, *Briefings Bioinf.* 22 (2021).
- [2] V. Defraine, M. Fauvert, J. Michiels, Fighting bacterial persistence: current and emerging anti-persister strategies and therapeutics, *Drug Resist. Updates* 38 (2018) 12–26.
- [3] W. Kim, G.L. Hendricks, K. Tori, B.B. Fuchs, E. Mylonakis, Strategies against methicillin-resistant *Staphylococcus aureus* persisters, *Future Med. Chem.* 10 (2018) 779–794.
- [4] S. Helaine, A.M. Cheverton, K.G. Watson, L.M. Faure, S.A. Matthews, D.W. Holden, Internalization of *Salmonella* by macrophages induces formation of nonreplicating persisters, *Science* 343 (2014) 204–208.
- [5] N. Chowdhury, T.L. Wood, M. Martínez-Vázquez, R. García-Contreras, T.K. Wood, DNA-crosslinker cisplatin eradicates bacterial persister cells, *Biotechnol. Bioeng.* 113 (2016) 1984–1992.
- [6] Y. Hu, A.R.M. Coates, Enhancement by novel anti-methicillin-resistant *Staphylococcus aureus* compound HT61 of the activity of neomycin, gentamicin, mupirocin and chlorhexidine: in vitro and in vivo studies, *J. Antimicrob. Chemother.* 68 (2012) 374–384.
- [7] V. Defraine, J. Schuermans, B. Grymonprez, S.K. Govers, A. Aertsen, M. Fauvert, J. Michiels, R. Lavigne, Y. Briers, Efficacy of artilysin art-175 against resistant and persistent *Acinetobacter baumannii*, *Antimicrob. Agents Chemother.* 60 (2016) 3480–3488.
- [8] C.N. Marques, A. Morozov, P. Planzos, H.M. Zelaya, The fatty acid signaling molecule *cis*-2-decenolic acid increases metabolic activity and reverts persister cells to an antimicrobial-susceptible state, *Appl. Environ. Microbiol.* 80 (2014) 6976–6991.
- [9] X. Duan, X. Huang, X. Wang, S. Yan, S. Guo, A.E. Abdalla, C. Huang, J. Xie, L-Serine potentiates fluoroquinolone activity against *Escherichia coli* by enhancing endogenous reactive oxygen species production, *J. Antimicrob. Chemother.* 71 (2016) 2192–2199.
- [10] W. Chang, J. Liu, M. Zhang, H. Shi, S. Zheng, X. Jin, Y. Gao, S. Wang, A. Ji, H. Lou, Efflux pump-mediated resistance to antifungal compounds can be prevented by conjugation with triphenylphosphonium cation, *Nat. Commun.* 9 (2018) 5102.
- [11] Y. Ye, T. Zhang, H. Yuan, D. Li, H. Lou, P. Fan, Mitochondria-targeted lupane triterpenoid derivatives and their selective apoptosis-inducing anticancer mechanisms, *J. Med. Chem.* 60 (2017) 6353–6363.
- [12] L. Leanza, M. Romio, K.A. Becker, M. Azzolini, L. Trentin, A. Managò, E. Venturini, A. Zaccagnino, A. Mattarei, L. Carraretto, A. Urbani, S. Kadow, L. Biasutto, V. Martini, F. Severini, R. Peruzzo, V. Trimarco, J.H. Egberts, C. Hauser, A. Visentin, G. Semenzato, H. Kalthoff, M. Zoratti, E. Gulbins, C. Paradisi, I. Szabo, Direct pharmacological targeting of a mitochondrial ion channel selectively kills tumor cells in vivo, *Cancer Cell* 31 (2017) 516–531.e510.
- [13] T. Li, X. He, W. Tao, R. Zhang, Q. He, H. Gong, Y. Liu, D. Luo, M. Zhang, C. Zou, S. L. Zhang, Y. He, Development of membrane-targeting TPP(+)–chloramphenicol conjugates to combat methicillin-resistant *staphylococcus aureus* (MRSA) infections, *Eur. J. Med. Chem.* 264 (2024) 115973.
- [14] S. Kang, K. Sunwoo, Y. Jung, J.K. Hur, K.H. Park, J.S. Kim, D. Kim, Membrane-targeting triphenylphosphonium functionalized ciprofloxacin for methicillin-resistant *Staphylococcus aureus* (MRSA), *Antibiotics (Basel, Switzerland)* 9 (2020).
- [15] K.A. Scott, P.B. Cox, J.T. Njardarson, Phenols in pharmaceuticals: analysis of a recurring motif, *J. Med. Chem.* 65 (2022) 7044–7072.
- [16] R. Najafloo, M. Behyari, R. Imani, S. Nour, A mini-review of Thymol incorporated materials: applications in antibacterial wound dressing, *J. Drug Deliv. Sci. Technol.* 60 (2020) 101904.
- [17] S. Zhao, Z.P. Wang, Z. Lin, G. Wei, X. Wen, S. Li, X. Yang, Q. Zhang, C. Jing, Y. Dai, J. Guo, Y. He, Drug repurposing by siderophore conjugation: synthesis and biological evaluation of siderophore-methotrexate conjugates as antibiotics, *Angew. Chem.* 61 (2022) e202204139.
- [18] S. Karnakanti, Z.L. Zang, S. Zhao, P.L. Shao, P. Hu, Y. He, Palladium-catalyzed oxidative arylacetoxylation of alkenes: synthesis of indole and indoline derivatives, *Chem. Commun.* 53 (2017) 11205–11208.
- [19] H. Peng, B. Xie, X. Yang, J. Dai, G. Wei, Y. He, Pillar[5]arene-based, dual pH and enzyme responsive supramolecular vesicles for targeted antibiotic delivery against intracellular MRSA, *Chem. Commun.* 56 (2020) 8115–8118.
- [20] Y. Zhong, X. He, W. Tao, J. Feng, R. Zhang, H. Gong, Z. Tang, C. Huang, Y. He, 2,4-Diacetylphloroglucinol (DAPG) derivatives rapidly eradicate methicillin-resistant *staphylococcus aureus* without resistance development by disrupting membrane, *Eur. J. Med. Chem.* 261 (2023) 115823.
- [21] Z. Lin, X. Xu, S. Zhao, X. Yang, J. Guo, Q. Zhang, C. Jing, S. Chen, Y. He, Total synthesis and antimicrobial evaluation of natural albomycins against clinical pathogens, *Nat. Commun.* 9 (2018) 3445.
- [22] X. Yang, B. Xie, H. Peng, G. Shi, B. Sreenivas, J. Guo, C. Wang, Y. He, Eradicating intracellular MRSA via targeted delivery of lysostaphin and vancomycin with mannose-modified exosomes, *J. Contr. Release : official journal of the Controlled Release Society* 329 (2021) 454–467.
- [23] Z. Tang, J. Feng, S.R. Rowthu, C. Zou, H. Peng, C. Huang, Y. He, Uncovering the anti-biofilm activity of Iliciculin B against *Staphylococcus aureus*, *Biochem. Biophys. Res. Commun.* 684 (2023) 149138.
- [24] D.M.P. De Oliveira, B.M. Forde, T.J. Kidd, P.N.A. Harris, M.A. Schembri, S. A. Beatson, D.L. Paterson, M.J. Walker, Antimicrobial resistance in ESKAPE pathogens, *Clin. Microbiol. Rev.* 33 (2020).
- [25] L.S. Khailova, P.A. Nazarov, N.V. Sumbatyan, G.A. Korshunova, T.I. Rokitskaya, V. I. Dedukhova, Y.N. Antonenko, V.P. Skulachev, Uncoupling and toxic action of alkyltriphenylphosphonium cations on mitochondria and the bacterium *Bacillus subtilis* as a function of alkyl chain length, *Biochemistry. Biokhimiia* 80 (2015) 1589–1597.
- [26] R.A. Smith, V.J. Adlam, F.H. Blaikie, A.R. Manas, C.M. Porteous, A.M. James, M. F. Ross, A. Logan, H.M. Cochemé, J. Trnka, T.A. Prime, I. Abakumova, B.A. Jones, A. Filipovska, M.P. Murphy, Mitochondria-targeted antioxidants in the treatment of disease, *Ann. N. Y. Acad. Sci.* 1147 (2008) 105–111.
- [27] S. Bai, J. Wang, K. Yang, C. Zhou, Y. Xu, J. Song, Y. Gu, Z. Chen, M. Wang, C. Shoen, B. Andrade, M. Cynamon, K. Zhou, H. Wang, Q. Cai, E. Oldfield, S. C. Zimmerman, Y. Bai, X. Feng, A polymeric approach toward resistance-resistant antimicrobial agent with dual-selective mechanisms of action, *Sci. Adv.* 7 (2021).
- [28] Y.N. Antonenko, M. Jedrzejczyk, T.I. Rokitskaya, L.S. Khailova, E.A. Kotova, A. Huczynski, Rate of translocation across lipid bilayer of triphenylphosphonium-linked salinomycin derivatives contributes significantly to their K(+)/H(+) exchange activity on membranes, *Bioelectrochemistry* 145 (2022) 108089.
- [29] K. Lu, W. Hou, X.F. Xu, Q. Chen, Z. Li, J. Lin, W.M. Chen, Biological evaluation and chemoproteomics reveal potential antibacterial targets of a cajaninstilbene-acid analogue, *Eur. J. Med. Chem.* 188 (2020) 112026.
- [30] K. Wang, W. Dang, J. Yan, R. Chen, X. Liu, W. Yan, B. Zhang, J. Xie, J. Zhang, R. Wang, Membrane perturbation action mode and structure-activity relationships of Protonectin, a novel antimicrobial peptide from the venom of the neotropical social wasp *Agelaea pallipes pallipes*, *Antimicrob. Agents Chemother.* 57 (2013) 4632–4639.
- [31] B. Luan, S. Zhou, D. Wang, R. Zhou, Detecting interactions between nanomaterials and cell membranes by synthetic nanopores, *ACS Nano* 11 (2017) 12615–12623.
- [32] J. Wainwright, G. Hobbs, I. Nakouti, Persister cells: formation, resuscitation and combative therapies, *Arch. Microbiol.* 203 (2021) 5899–5906.
- [33] W. Kim, W. Zhu, G.L. Hendricks, D. Van Tyne, A.D. Steele, C.E. Keohane, N. Fricke, A.L. Conery, S. Shen, W. Pan, K. Lee, R. Rajamuthiah, B.B. Fuchs, P.M. Vlahovska,

- W.M. Wuest, M.S. Gilmore, H. Gao, F.M. Ausubel, E. Mylonakis, A new class of synthetic retinoid antibiotics effective against bacterial persisters, *Nature* 556 (2018) 103–107.
- [34] C. Zhong, N. Zhu, Y. Zhu, T. Liu, S. Gou, J. Xie, J. Yao, J. Ni, Antimicrobial peptides conjugated with fatty acids on the side chain of D-amino acid promises antimicrobial potency against multidrug-resistant bacteria, *Eur. J. Pharmaceut. Sci. : official journal of the European Federation for Pharmaceutical Sciences* 141 (2020) 105123.
- [35] G. Cheng, M. Hardy, J. Zielonka, K. Weh, M. Zielonka, K.A. Boyle, M. Abu Eid, D. McAllister, B. Bennett, L.A. Kresty, M.B. Dwinell, B. Kalyanaraman, Mitochondria-targeted magnolol inhibits OXPHOS, proliferation, and tumor growth via modulation of energetics and autophagy in melanoma cells, *Cancer treatment and research communications* 25 (2020) 100210.
- [36] S. Lin, J. Liu, H. Li, Y. Liu, Y. Chen, J. Luo, S. Liu, Development of highly potent carbazole amphiphiles as membrane-targeting antimicrobials for treating gram-positive bacterial infections, *J. Med. Chem.* 63 (2020) 9284–9299.
- [37] B.P. Conlon, S.E. Rowe, A.B. Gandy, A.S. Nuxoll, N.P. Donegan, E.A. Zalis, G. Clair, J.N. Adkins, A.L. Cheung, K. Lewis, Persister formation in *Staphylococcus aureus* is associated with ATP depletion, *Nature microbiology* 1 (2016).
- [38] B.P. Conlon, E.S. Nakayasu, L.E. Fleck, M.D. LaFleur, V.M. Isabella, K. Coleman, S. N. Leonard, R.D. Smith, J.N. Adkins, K. Lewis, Activated ClpP kills persisters and eradicates a chronic biofilm infection, *Nature* 503 (2013) 365–370.
- [39] C.Z. Chen, S.L. Cooper, Interactions between dendrimer biocides and bacterial membranes, *Biomaterials* 23 (2002) 3359–3368.
- [40] J.K. Martin 2nd, J.P. Sheehan, B.P. Brattton, G.M. Moore, A. Mateus, S.H. Li, H. Kim, J.D. Rabinowitz, A. Typas, M.M. Savitski, M.Z. Wilson, Z. Gitai, A dual-mechanism antibiotic kills gram-negative bacteria and avoids drug resistance, *Cell* 181 (2020), 1518–1532.e1514.
- [41] E.J. Culp, N. Waglechner, W. Wang, A.A. Fiebig-Comyn, Y.P. Hsu, K. Koteva, D. Sychantha, B.K. Coombes, M.S. Van Nieuwenhze, Y.V. Brun, G.D. Wright, Evolution-guided discovery of antibiotics that inhibit peptidoglycan remodelling, *Nature* 578 (2020) 582–587.
- [42] Z. Lai, P. Tan, Y. Zhu, C. Shao, A. Shan, L. Li, Highly stabilized α -helical coiled coils kill gram-negative bacteria by multicomplementary mechanisms under acidic condition, *ACS Appl. Mater. Interfaces* 11 (2019) 22113–22128.
- [43] J. Li, S. Liu, R. Lakshminarayanan, Y. Bai, K. Pervushin, C. Verma, R.W. Beuerman, Molecular simulations suggest how a branched antimicrobial peptide perturbs a bacterial membrane and enhances permeability, *Biochim. Biophys. Acta Biomembr.* 1828 (2013) 1112–1121.
- [44] K. Murzyn, T. Rog, M. Pasenkiewicz-Gierula, Phosphatidylethanolamine-phosphatidylglycerol bilayer as a model of the inner bacterial membrane, *Biophys. J.* 88 (2005) 1091–1103.
- [45] J. Li, S. Liu, J.J. Koh, H. Zou, R. Lakshminarayanan, Y. Bai, K. Pervushin, L. Zhou, C. Verma, R.W. Beuerman, A novel fragment based strategy for membrane active antimicrobials against MRSA, *Biochim. Biophys. Acta* 1848 (2015) 1023–1031.
- [46] Z. Si, J. Li, L. Ruan, S. Reghu, Y.J. Ooi, P. Li, Y. Zhu, P.T. Hammond, C.S. Verma, G. C. Bazan, K. Pethé, M.B. Chan-Park, Designer co-beta-peptide copolymer selectively targets resistant and biofilm Gram-negative bacteria, *Biomaterials* 294 (2023) 122004.
- [47] R. Mani, S.D. Cady, M. Tang, A.J. Waring, R.I. Lehrer, M. Hong, Membrane-dependent oligomeric structure and pore formation of a beta-hairpin antimicrobial peptide in lipid bilayers from solid-state NMR, *Proc. Natl. Acad. Sci. U. S. A.* 103 (2006) 16242–16247.
- [48] S. Bailleul, K. Dedecker, P. Cnudde, L. Vanduyfhuys, M. Waroquier, V. Van Speybroeck, Ab initio enhanced sampling kinetic study on MTO ethene methylation reaction, *J. Catal.* 388 (2020) 38–51.
- [49] X. Yang, C. Zhang, X. Yang, Z. Xu, Free energy reconstruction/decomposition from WHAM, force integration and free energy perturbation for an umbrella sampling simulation, *Chem. Phys.* 565 (2023) 111736.
- [50] J. Huang, S. Rauscher, G. Nawrocki, T. Ran, M. Feig, B.L. de Groot, H. Grubmüller, A.D. MacKerell, CHARMM36m: an improved force field for folded and intrinsically disordered proteins, *Nat. Methods* 14 (2017) 71–73.
- [51] S. Jo, T. Kim, V.G. Iyer, W. Im, CHARMM-GUI: a web-based graphical user interface for CHARMM, *J. Comput. Chem.* 29 (2008) 1859–1865.
- [52] K. Kholmurodov, W. Smith, K. Yasuoka, T. Darden, T. Ebisuzaki, A smooth-particle mesh Ewald method for DL_POLY molecular dynamics simulation package on the Fujitsu VPP700, *J. Comput. Chem.* 21 (2000) 1187–1191.
- [53] M. Montal, P. Mueller, Formation of bimolecular membranes from lipid monolayers and a study of their electrical properties, *Proc. Natl. Acad. Sci. U.S.A.* 69 (1972) 3561–3566.
- [54] B. Luan, G. Stolovitzky, An electro-hydrodynamics-based model for the ionic conductivity of solid-state nanopores during DNA translocation, *Nanotechnology* 24 (2013) 195702.
- [55] M.A.T. Blaskovich, A.M. Kavanagh, A.G. Elliott, B. Zhang, S. Ramu, M. Amado, G. J. Lowe, A.O. Hinton, D.M.T. Pham, J. Zuegg, N. Beare, D. Quach, M.D. Sharp, J. Poglino, A.P. Rogers, D. Lyras, L. Tan, N.P. West, D.W. Crawford, M.L. Peterson, M. Callahan, M. Thurn, The antimicrobial potential of cannabidiol, *Commun. Biol.* 4 (2021) 7.